Supporting Information

Upgraded Closed-loop Recycling of PET for High-voltage Solid-state Electrolytes and Their Critical Li^+ Transport

Minghui Wang,[a#] Xihui Li,[a#] Peng Zhang,[a#] Zhaoxu Wang,[b#] Shu-Meng Hao,[a*] Shuang He,[a] Xuan Qin,[a*] Guangmin Zhou,[c*] Weidong Zhou[a*]

[a] Beijing Advanced Innovation Center for Soft Matter Science and Engineering, State Key Laboratory of Organic-Inorganic Composites, Beijing University of Chemical Technology, Beijing 100029, China [b] Key Laboratory of Theoretical Organic Chemistry and Functional Molecule of Ministry of Education, Hunan University of Science and Technology, Hunan, 411201, China

[c] Shenzhen Geim Graphene Center, Tsinghua Shenzhen International Graduate School, Tsinghua University, Shenzhen, China

*email: haosm@buct.edu.cn, qinxuan@mail.buct.edu.cn, guangminzhou@sz.tsinghua.edu.cn, zhouwd@mail.buct.edu.cn

These authors contributed equally: Minghui Wang, Xihui Li, Peng Zhang, Zhaoxu Wang

Methods

Materials

1,5-pentanediol (C5-diol, >99% purity), zinc acetate (>99% purity), dimethyl oxalate (DMOA, >99% purity), 1,9-nonanediol (C9-diol, >99% purity), dimethyl terephthalate (DMT, >99% purity), ethylene carbonate (EC, >99% purity), dimethyl carbonate (DMC, >99% purity), diethyl carbonate (DEC, >99% purity) and fluoroethylene carbonate (FEC, >99% purity) were purchased from Tokyo Chemical Industry. N-methyl-2pyrrolidone (NMP, >99% purity), dimethyl sulfoxide (DMSO, >99% purity), acetonitrile (CH_3CN, >99.5% purity), titanium isopropoxide (>98% purity), trifluoroacetic anhydride (98% purity), acetone (>99% purity) and isopropyl ether (IPE, >99% purity) were bought from Aladdin. Lithium bis(trifluoromethanesulfonyl)imide (LiTFSI, >99.9% purity) was obtained from YACOO. Poly(vinylidene fluoride) (PVDF, >99% purity) was purchased from Alfa Aesar. Poly(ethylene glycol) methyl ether methacrylate (PEGMA) was sourced from Sigma-Aldrich.

Syntheses of BAET, BHETA and BHET

Waste PET pieces, C5-diol, zinc acetate and NMP with a weight ratio of 1:6:0.05:1.5 were placed in a 250 mL three-necked flask. The mixture was heated at 170 ^{o}C for 4 h under nitrogen flow and cooled to room temperature. After adding an additional portion of zinc acetate (weight ratio of 0.05 relative to PET), the mixture was then heated again at 170 ^{o}C for 4 h. The obtained suspension was dissolved in deionized water under stirring at 80 ^{o}C to filtrate off the undepolymerized PET and oligomers. Then BAET was obtained through crystallization at 0~4 ^{o}C in water, followed by filtration. The synthesis procedures of BHETA and BHET were similar to those of BAET, while BHETA and BHET were prepared through ammonolysis and alcoholysis of PET by ethanolamine and ethylene glycol, respectively.

Preparation and characterization of BHETA and BHET single crystals

BHETA was dissolved in DMSO at a weight ratio of 1:10, and then mixed with deionized water to obtain the saturated solution at room temperature. The crystals were obtained through slow evaporation of the solvents. The growth process of BHET crystal was similar to that of BHETA, but BHET was dissolved in methanol and then mixed with deionized

water. Gemin E single-crystal X-ray Diffractometer was used to test the single crystal structures of BHETA and BHET.

Syntheses of PTOs, PTAs, PTs and POEs

BAET, DMOA, C5-diol with the molar ratio of 1:3:2.075 were placed in a 100 mL threenecked flask, and titanium isopropoxide (1 mol% relative to DMOA) was added in the mixture. The mixture was sequentially heated at 100 ^{o}C for 2 h, 110 ^{o}C for 1 h, 120 ^{o}C for 1 h and then 145 ^{o}C for 12 h under N_2 flow. Afterwards, the reaction was maintained at 145 ^{o}C for 4 h under vacuum, followed by increasing the temperature to 160 ^{o}C for 3 h and then 180 ^{o}C for 1 h under vacuum. After cooling to room temperature, the polymer was dissolved in CH_2Cl_2, and titanium isopropoxide was removed by extraction using deionized water. The polymer was obtained by drying. To fluorinate the terminal group, the dried polymer was dissolved in anhydrous CH_2Cl_2 under a N_2 atmosphere, and then trifluoroacetic anhydride (polymer: trifluoroacetic anhydride = 1:6, molar ratio) was added to the solution and stirred at 0 ^{o}C for 2 h. After that, the reaction was maintained at 25 ^{o}C for 8 h and then 50 ^{o}C for 2 h. The reactant solution was added dropwise into cold methanol, and the resulting precipitate was dried under vacuum to produce PTO-C5 (1:3), also abbreviated as PTO-C5.

The PTO-C5 (1:6) and PTO-C5 (1:1) were synthesized following the same procedure as PTO-C5 (1:3), expect that the molar ratio of BAET:DMOA:(C5-diol) was changed to 1:6:5.15 and 1:1:0.025, respectively. PTO-C5 (2:1) was also synthesized as the same procedure, but DMT was used to replace BAET, and the molar ratio of DMT:DMOA:C5diol is 2:1:3.075 with 1 mol% (relative to DMT+DMOA) of titanium isopropoxide. The preparation method of PTO-C9 was similar to that of PTO-C5 (1:3), but using 1,9nonanediol (C9-diol) to replace C5-diol. The synthesis procedure of PTA-C9 was similar to that of PTO-C9, but using BHETA instead of BAET.

Additionally, PT-C5 (or PT-C9) was synthesized by the reaction between DMT and C5diol (or DMT and C9-diol) in the molar ratio of 1:1.025 with 1 mol% (relative to DMT) of titanium isopropoxide, and the preparation procedure is the same as that of PTO-C5 (1:3). POE-C5 (or POE-C9) was synthesized by the reaction between DMOA and C5-diol (or DMOA and C9-diol) in the molar ratio of 1:1.025 with 1 mol% (relative to DMOA) of titanium isopropoxide, and the preparation procedure is the same as that of PTO-C5 (1:3).

Preparation of QSSEs

The polymer and LiTFSI were dissolved in CH_3CN, and the solution was then dropped onto glass-fiber membranes. After evaporating CH_3CN, the membranes were placed under vacuum at 40 ^oC for 10 h. After transferring into glove box, the membranes were infiltrated with a certain amount of liquid (5 wt%–30 wt% relative to polymer+liquid+LiTFSI) in the (polymer+liquid):LiTFSI weight ratio of 2.5:1, and then the membranes were sealed and stored for 8 h to ensure the fully diffusion of liquid.

Positive electrode preparation and coin cell assembly

The NCM85 or LMFP powder (75 wt%) was first ground with carbon black (8 wt%). The mixture together with 15 wt% of solid polymer electrolyte (polymer:LiTFSI = 2.5:1, weight ratio) were dispersed into PVDF (2 wt%) solution in NMP. The obtained suspension was mixed in a Thinky mixer to form a uniform slurry, which was coated on Al foil and dried under vacuum at 65 ^oC for 24 h, with an active material loading of ~5 mg cm^{-2}.

The coin cells were assembled with NCM85 or LMFP positive electrodes and Li-metal negative electrodes in 2032 stainless steel cases, using PTO-C5 or PTO-C9 based QSSEs as electrolytes. All coin cells were assembled in a glovebox filled with argon (H_2O < 0.1 ppm, O_2 < 0.1 ppm).

Pouch cell assembly

Si-C and NCM90 were used as the negative electrode and positive electrode for a 5.0 Ah multilayer dry pouch cell. The PTO-C9 and LiTFSI were blended with the mixed liquid of EC+DEC+FEC (1:1:1, weight ratio), giving 10 g of PTO-C9-Li-L electrolyte ((polymer+liquid):LiTFSI=2.5:1, weight ratio; liquid content: 30 wt%). Afterwards, additional 6.7 g DEC was added into PTO-C9-Li-L to form a flowable liquid electrolyte, which was then injected into the dry pouch cell, followed by heat sealing. The cell was rested for 24 h for fully infiltration of the electrolyte. The first cycle was chargeddischarged at 0.02C as the formation cycle, and then extra DEC was pumped out, followed by cutting off the air pocket and sealing, with the final cell weight of 51.37 g.

Characterizations

The gel permeation chromatography (GPC) analysis was performed using a Waters GPC 1515 system. The NMR spectra were obtained using a Bruker AVANCE III 400 MHz spectrometer. The single crystal structures of BHETA and BHET were determined using a

single-crystal X-ray diffraction (SXRD, Gemin E). The XRD spectra were obtained using a D8 Discover (Bruker) with Cu Ka radiation (2θ=5–80°). The free volume of polymers was determined by positron annihilation lifetime spectrometer (PALS). The differential scanning calorimetry (DSC) was performed using a NETZSCH DSC 214 Polyma with a heating rate of 20 °C min^{-1} in N_2 atmosphere. The thermogravimetric analysis (TGA) was conducted on a NETZSCH TG209F3 from 40 to 600 °C at a heating rate of 10 °C min^{-1} in N_2 atmosphere. The FT-IR spectra were obtained by a Nicolet 6700 FT-IR spectrometer. Raman spectra were obtained by a Raman spectrometer (inVia Reflex). The micromorphology of the interface layers on Li metal was observed using a JSM-7800 field emission scanning electron microscope (SEM). The interfacial chemistry of the polymer membranes and Li-foil surface before and after cycling was analyzed using a Thermo Axis Supra high-resolution XPS.

Electrochemical measurements

The ionic conductivities of various electrolytes at different temperatures (ranging from 25 to 75 °C) were calculated from electrochemical impedance spectroscopy (EIS) plots. The stainless steel//stainless steel coin cells were assembled, and the EIS plots were conducted in the frequency region of 1.0 MHz to 0.1 Hz on a Solartron Analytical system with an amplitude of 10 mV. The ionic conductivities (σ) were calculated using the following equation:

$$\sigma = L/RS \qquad (4)$$

where L is defined as the thickness of the QSSE membranes, R represents the resistance of the bulk electrolyte, and S stands for the surface area of the electrode.

The Li^+ transference numbers (t_{Li^+}) were derived by combining AC impedance and direct current (DC) polarization techniques using a Li//Li cell. The t_{Li^+} was calculated according to the following equations:

$$t_{Li+} = \frac{I_s(\Delta V - I_0 R_0)}{I_0(\Delta V - I_s R_s)}$$

Where ΔV is the polarization potential (10 mV), I_0 and I_s are the initial current and steady current, respectively, during the polarization process. R_0 and R_s are the initial and final impedance of electrode/electrolyte interface, respectively.

Linear scanning voltammetry (LSV) with Li//stainless steel cells was performed on a Solartron Analytical electrochemical workstation to determine the electrochemical stability window, scanning the potential from OCV to 5.5 V at a rate of 0.5 mV s^{-1}. Cyclic voltammetry (CV) measurements with Li//stainless steel cells were conducted on the same system at a constant scan rate of 0.3 mV s^{-1}. The electrochemical float test with Li//NCM85 cells was performed using a LAND CT3002A battery testing system (Wuhan, China). The Li//NCM85 cell was first charged to 4.0 V via constant current, followed by stepwise voltage increments of 0.1 V (from 4.1 V to 5.0 V), with each voltage stage maintained under constant voltage charging for 10 hours.

The galvanostatic charge/discharge tests of Li//Li, Li//NCM85 and Li//LMFP coin cells were carried on the LAND battery test system (CT3002A, Wuhan, China). The galvanostatic cycling of Li//Li cells was performed at 0.2 mAh cm^{-2} and 25 ^{o}C. The cycling performance of Li//NCM85 and Li//LMFP cells were tested at 30 ^{o}C, at a current density of 0.5C after activation at 0.1C. The galvanostatic charge/discharge tests of the pouch cells were performed on a LAND battery testing system (CT3002A, Wuhan, China) at 30 °C. The pouch cells were charged and discharged within a voltage range of 2.5–4.25 V at a current density of 0.1C after formation at 0.02C.

Calculation of battery specific energy

Battery specific energy refers to the amount of energy (Wh) that a battery can release per unit mass (kg), which can be calculated by the following equation:

$$\text{Battery energy density (Wh kg}^{-1}\text{)} = \text{discharge energy (Wh)/battery mass (kg)} \quad (5)$$

In this study, the energy density of the pouch cell was determined to be 364 Wh kg^{-1}. This value was calculated based on an energy of 18.7 Wh and a battery mass of 51.37 g.

Theoretical Simulation and Calculation.

All these density functional theory calculations were accomplished by Gaussian 16 software.[1] The geometry structures of the monomers and their complex were fully optimized by the B3LYP method with 6-31++G(d, p) basis set.[2,3] Vibrational frequency analyses were conducted to ensure no imaginary frequency existing in each optimized structure. The intermolecular interaction energy (ΔE) was calculated according to the following equation:

$$\Delta E = E_{complex} - E_A - 8E_B \quad (6)$$

Where $E_{complex}$ is the total energies of complex; E_A and E_B are the energies of PTO-C5 and solvent molecule (EC, DMC, DEC).

Molecular dynamics (MD) simulations were conducted utilizing the GROMACS package.[4] The Optimized Potentials for Liquid Simulations All Atom force fields[5] parameters, combined with Restrained ElectroStatic Potential (RESP) charges[6] derived from Multiwfn[7] were used for EC, DEC and polymer chains. To achieve model simplification, the oxalate–$(CH_2)_5$–oxalate segment and terephthalate–$(CH_2)_5$–oxalate segment at the molar ratio of 1:1 were used to represent PTO-C5, defined as OOTO1-1. The force field for $TFSI^-$ was accessed from previous study.[8] Initial system configurations were generated using PACKMOL.[9] Subsequent equilibration of the electrolyte system proceeded under NPT ensemble conditions (constant particle number, pressure, and temperature) at 600 K for 5 ns, followed by further equilibration at 298 K for 10 ns. A subsequent production run was performed within the NVT ensemble (constant particle number, volume, and temperature) at 298 K for 10 ns. Structural analysis of the electrolyte utilized trajectory data from the final 5 ns.

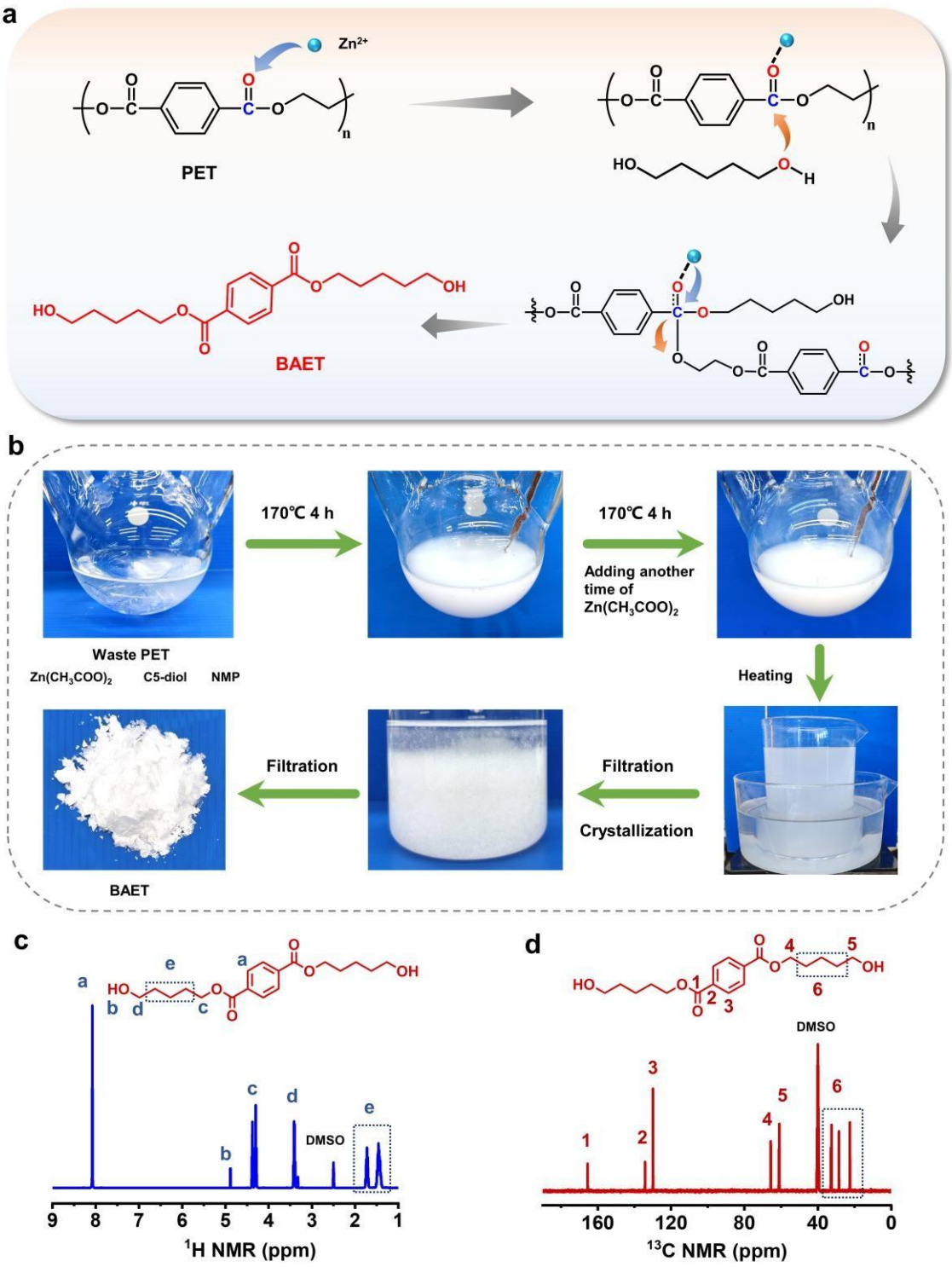

Fig. S1 (a) The alcoholysis mechanism of PET in the presence of $Zn(CH_3COO)_2$ catalyst. (b) Alcoholysis procedure of PET. (c) ^{1}H NMR and (d) ^{13}C NMR spectra of BAET.

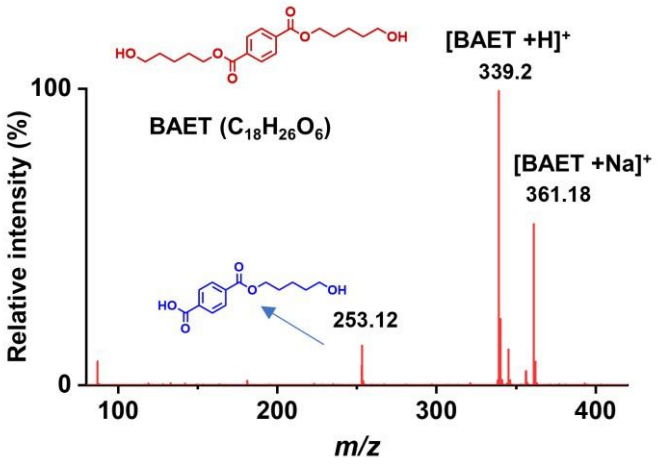

Fig. S2 Electrospray Ionization Mass Spectrometry (ESI-MS) of BAET.

The primary ion peak of BAET at *m/z* 339.2 corresponds to $[BAET+H]^+$, while the weaker ion peak at *m/z* 361.18 is attributed to $[BAET+Na]^+$, indicating the recovered BAET.

Table S1. Elemental analysis of BAET, BHET and BHETA.

Sample	Actual element content (wt%)				Theoretical element content (wt%)			
	C	H	N	S	C	H	N	S
BAET ($C_{18}H_{26}O_6$)	63.76	7.90	0.01	0.01	63.90	7.69	0	0
BHETA ($C_{12}H_{16}N_2O_4$)	56.35	6.33	10.96	0.01	57.14	6.34	11.11	0
BHET ($C_{12}H_{14}O_6$)	56.79	5.62	0.01	0.01	56.69	5.51	0	0

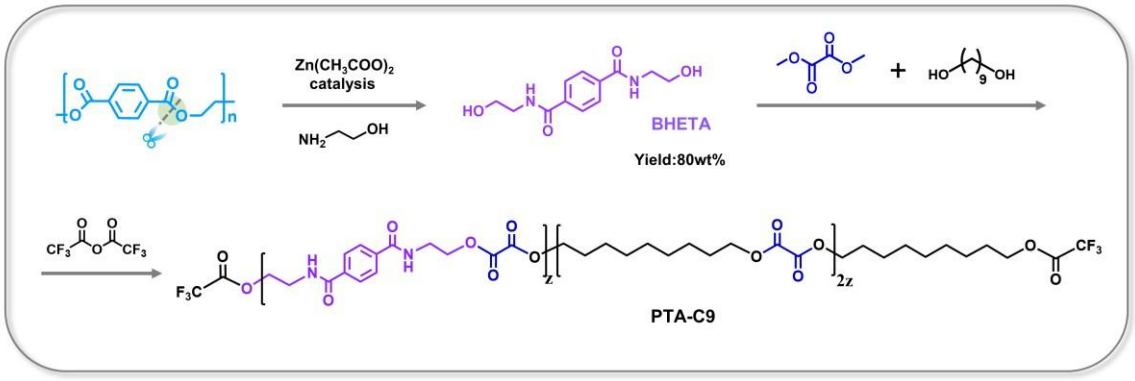

Fig. S3 The ammonolysis of PET by ethanolamine and the synthesis routes of PTA-C9.

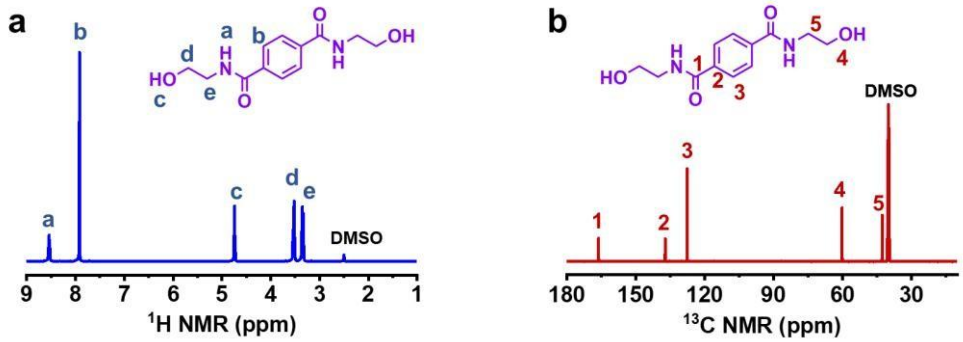

Fig. S4 (a) ^{1}H NMR and (b) ^{13}C NMR spectra of BHETA.

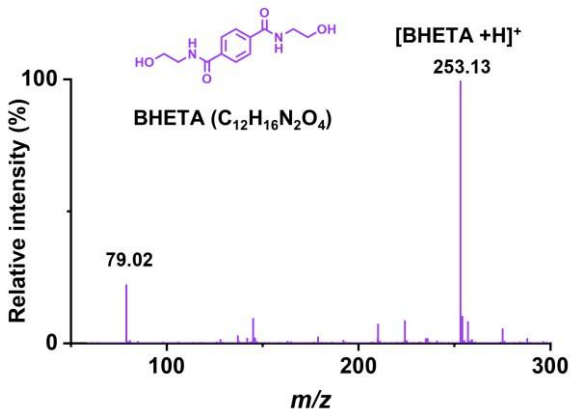

Fig. S5 Electrospray Ionization Mass Spectrometry (ESI-MS) of BHETA

The main ion peak of BHETA is observed at *m/z* 253.13 corresponding to the $[BHETA+H]^{+}$, indicating the generation of BHETA.

a

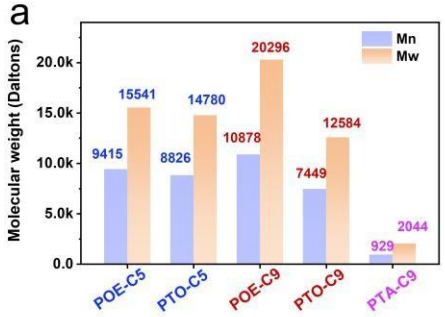

b

Samples	Mn	Mw	PDI
POE-C5	9415	15541	1.65
PTO-C5	8826	14780	1.67
POE-C9	10878	20296	1.86
PTO-C9	7449	12584	1.69

c

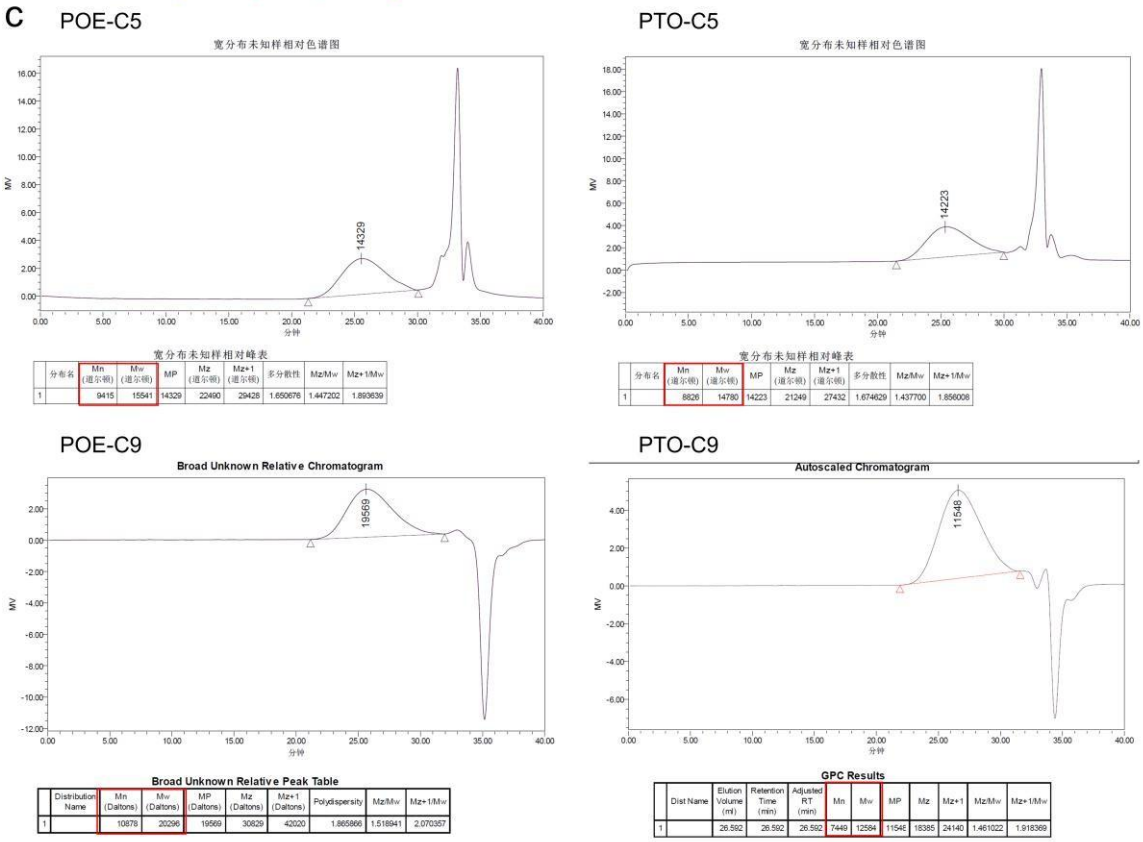

Fig. S6 (a) Mw and Mn values of POE, PTO and PTA-based polymers. (b) Mw, Mn and PDI values and (c) GPC curves and of POE-C5, PTO-C5, POE-C9 and PTO-C9.

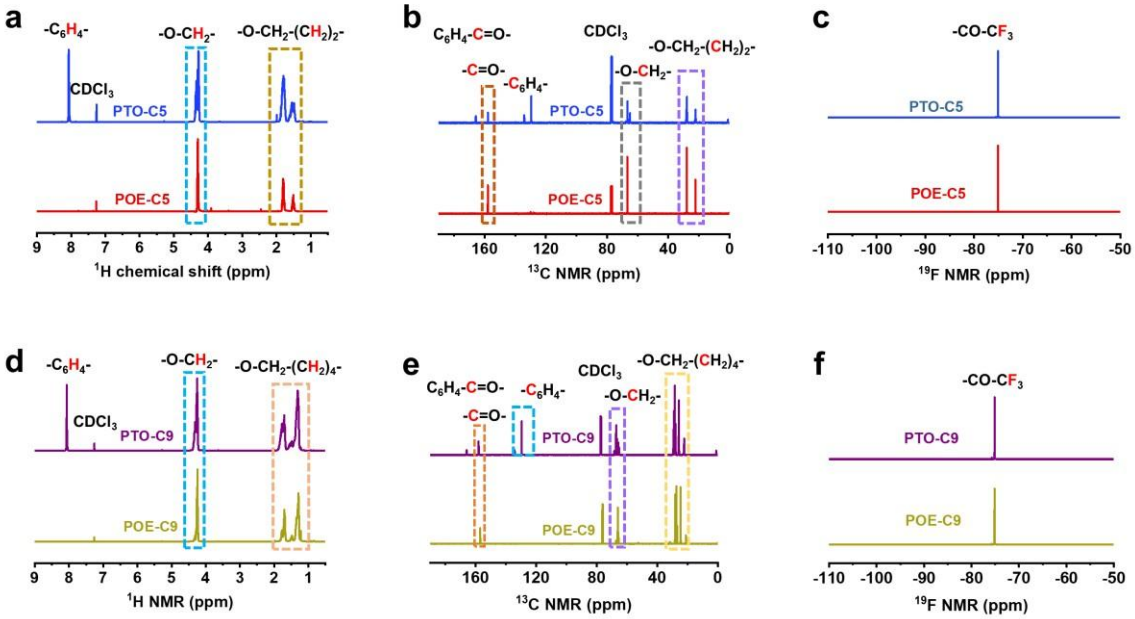

Fig. S7 (a) ^{1}H NMR, (b) ^{13}C NMR and (c) ^{19}F NMR spectra of POE-C5, PTO-C5 polymers. (d) ^{1}H NMR, (e) ^{13}C NMR and (f) ^{19}F NMR spectra of POE-C9 and PTO-C9 polymers (using $CDCl_3$ as solvent).

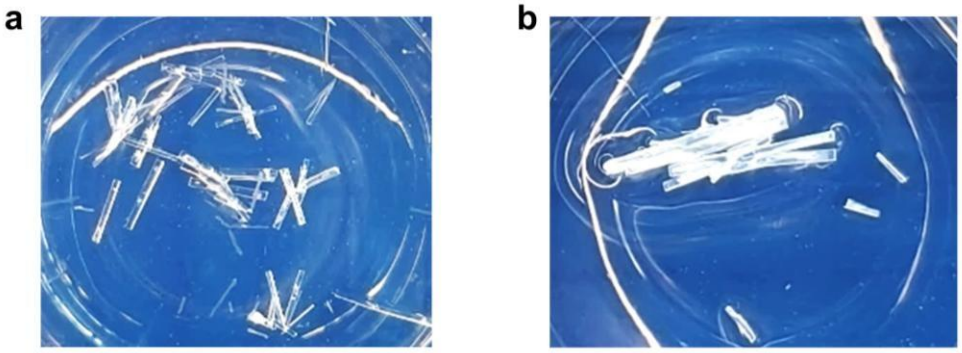

Fig. S8 Optic images of experimentally obtained (a) BHET and (b) BHETA single crystals.

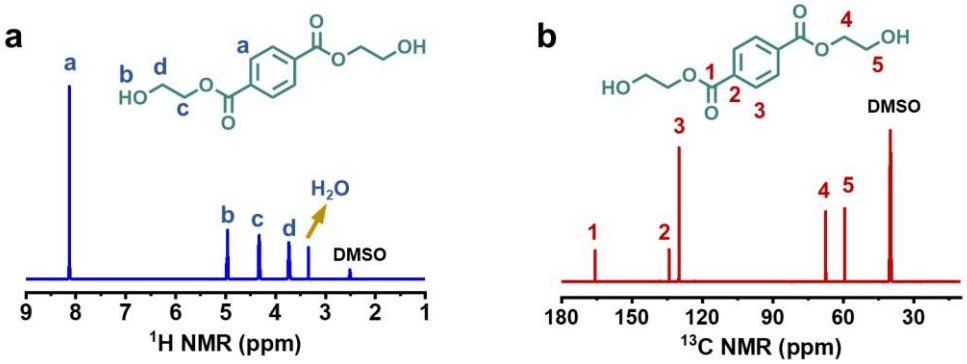

Fig. S9 (a) ^{1}H NMR and (b) ^{13}C NMR spectra of BHET.

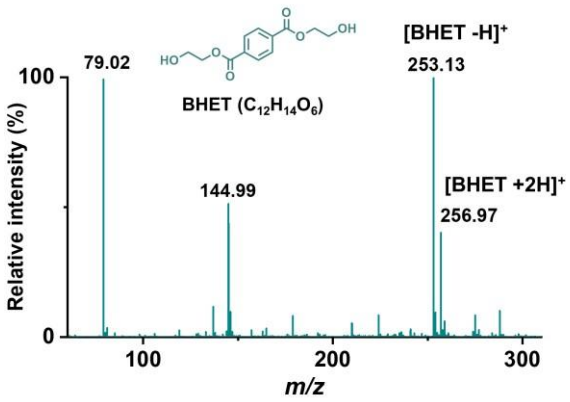

Fig. S10 Electrospray Ionization Mass Spectrometry (ESI-MS) of BHET.

The ion peak of BHET observed at *m/z* 253.13 corresponds to $[BHET-H]^+$, indicating the generation of BHET.

Table S2. Crystallographic data and structure refinement information of single crystal samples.

Sample	BHETA	BHET
Empirical formula	$C_{12}H_{16}N_2O_4$	$C_{12}H_{14}O_6$
Formula weight	252.27	254.23
Temperature/K	120.40(10)	119.00(10)
Crystal system	monoclinic	orthorhombic
Space group	P21/c	P212121
a/Å	4.9229(7)	5.6643(5)
b/Å	13.6267(9)	7.5093(6)
c/Å	8.8349(6)	26.967(2)
α/°	90.00	90.00
β/°	97.908(11)	90.00
γ/°	90.00	90.00
Volume/$Å^3$	587.03(10)	1147.03(16)
Z	2	4
ρcalc/mg mm^{-3}	1.427	1.427
μ/mm^{-1}	0.108	0.119
F(000)	268	536

Crystal size/mm^3	0.38×0.21×0.16	0.36×0.33×0.01
2Θ range for data collection	5.98 to 51.96°	6.22 to 51.94°
Index ranges	-6≤h≤5, -16≤k≤15, -10≤l≤8	-6 ≤h ≤6, -8≤ k≤ 9, -33≤l≤32
Reflections collected	2274	3724
Independent reflections	1122[R(int)=0.0281 (inf-0.9Å)]	2177[R(int)=0.0333 (inf-0.9Å)]
Data/restraints/parameters	1122/0/84	2177/0/165
Goodness-of-fit on F^2	1.063	1.030
Final R indexes [I>2σ (I) i.e. Fo>4σ (Fo)]	R1 =0.0407, wR2 =0.0887	R1 =0.0446, wR2 =0.0769
Final R indexes [all data]	R1 =0.0511, wR2 =0.0975	R1 =0.0578, wR2 =0.0844
Largest diff. peak/hole / e Å^{-3}	0.180/-0.194	0.175/-0.227
CCDC number	2359583	2359584

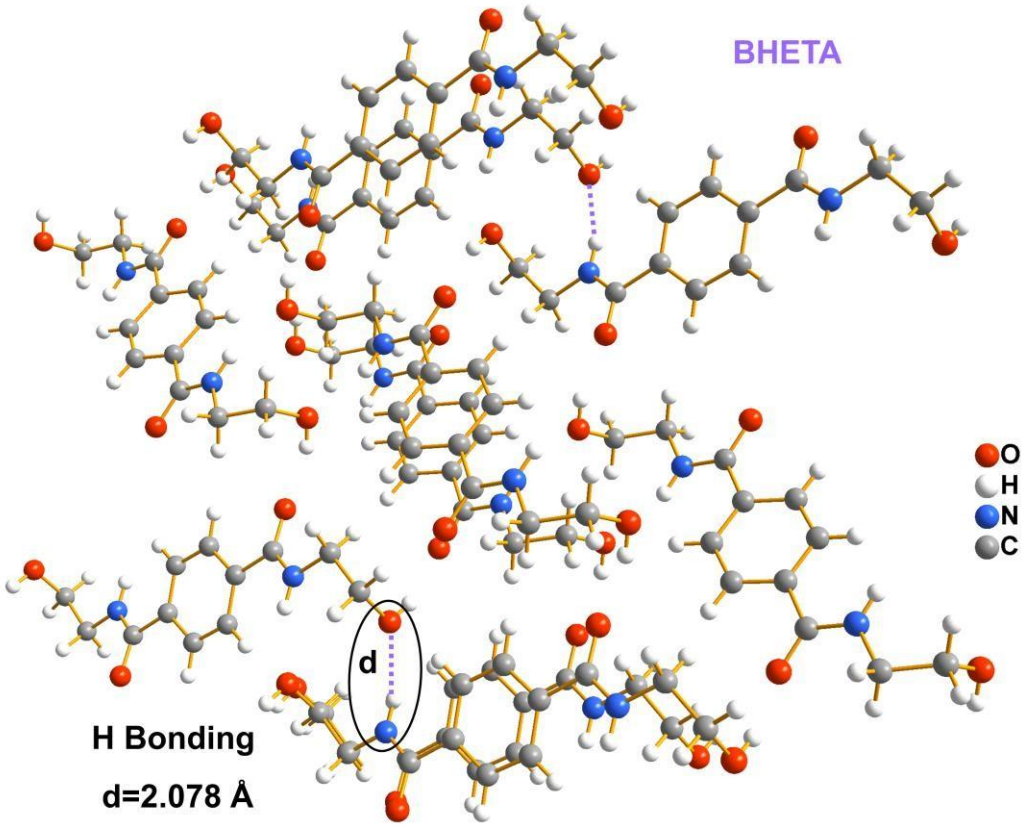

Fig. S11 Single-crystal structure of BHETA.

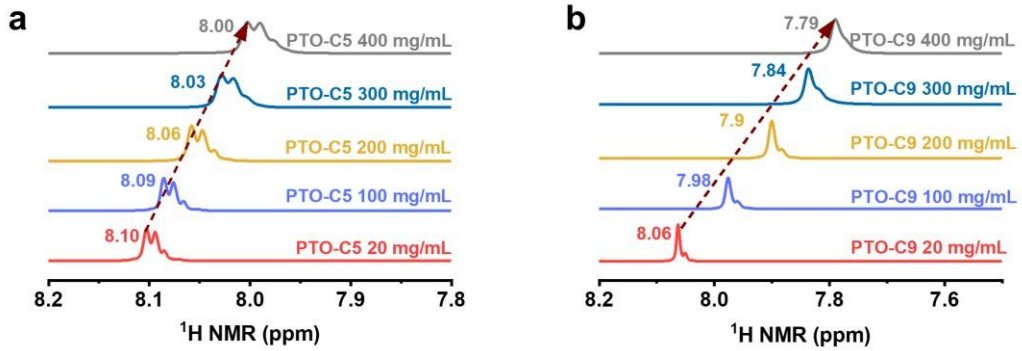

Fig. S12 ^{1}H NMR of (a) PTO-C5 and (b) PTO-C9 with various concentrations in $CDCl_3$.

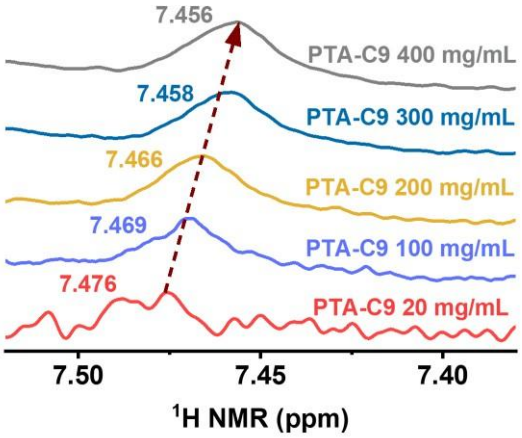

Fig. S13 ^{1}H NMR of PTA-C9 with various concentrations in DMSO-d_6.

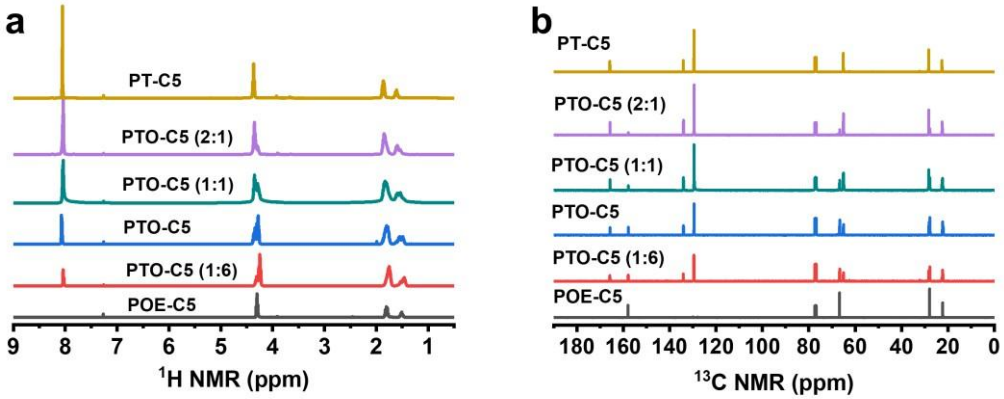

Fig. S14 (a) ^{1}H NMR and (b) ^{13}C NMR spectra of POE-C5, PTO-C5 (1:6), PTO-C5, PTOC5 (1:1), PTO-C5 (2:1) and PT-C5. The molar ratios of terephthalate to oxalate are fixed at 0:1, 1:6, 1:3, 1:1, 2:1 and 1:0, respectively.

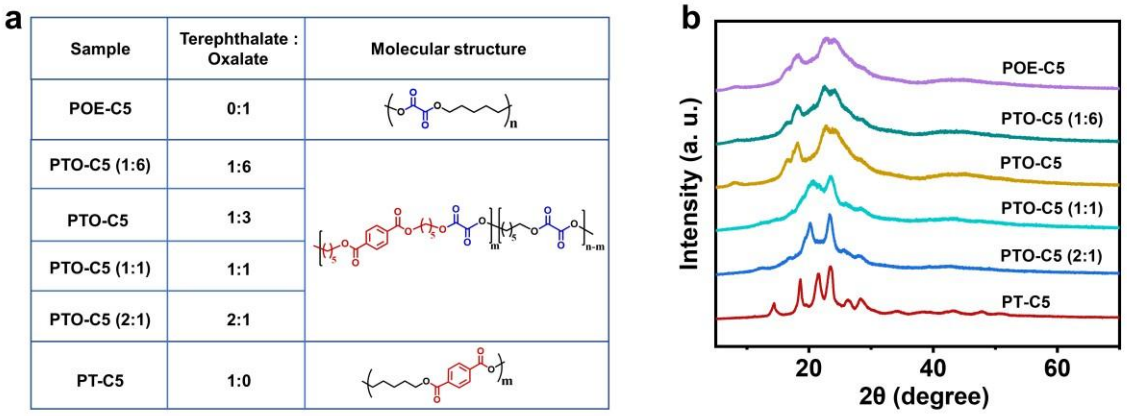

Fig. S15 (a) Molecular structures of polymers with different molar ratios of terephthalate to oxalate. (b) The XRD patterns of POE-C5, PTO-C5 (1:6), PTO-C5, PTO-C5 (1:1), PTOC5 (2:1) and PT-C5.

The molar ratios of terephthalate to oxalate are fixed at 0:1, 1:6, 1:3, 1:1, 2:1 and 1:0. POE-C5 (without terephthalate units) shows a broad diffraction peak and tends to be an amorphous state. By comparison, as the terephthalate:oxalate ratio increases from 0:1 to 1:0, the crystallinity of PTO-C5 gradually increases, and PT-C5 (without oxalate units) exhibits sharp diffraction peaks and high crystallinity, which can be ascribed to the π-π interactions between terephthalate units.

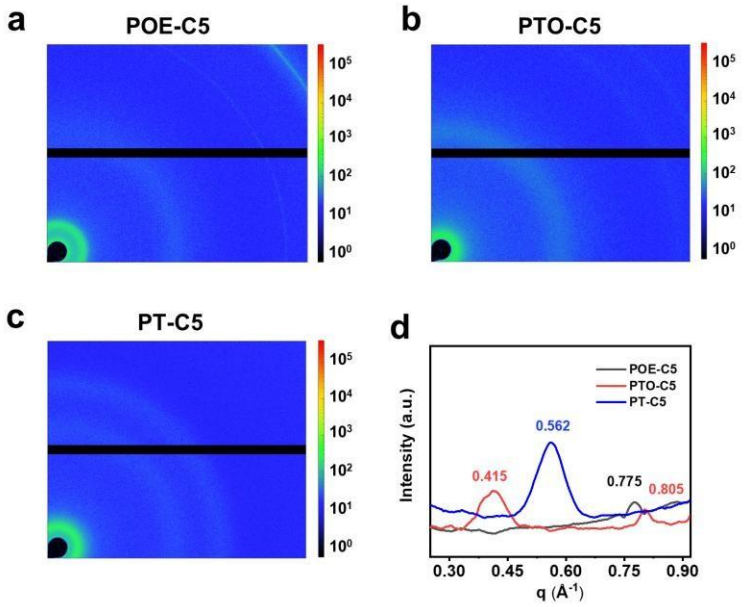

Fig. S16 (a-c) Small angle X-ray scattering (SAXS) patterns of POE-C5, PTO-C5 (terephthalate:oxalate = 1:3) and PT-C5. (d) SAXS profiles of POE-C5, PTO-C5 and PTC5, where the molar ratios of terephthalate to oxalate are fixed at 0:1, 1:3 and 1:0, respectively.

Table S3. Free volume testing results of PTO-C5-Li with various molar ratios of terephthalate to oxalate.

Sample	[a]τ_3 (ns)	[b]I_3 (%)	[c]R (Å)	[d]V_f (Å)$_3$	[e]f_v (%)
PTO-C5-Li (1:3)	4.22	13.8	4.41	360.30	4.97
PTO-C5-Li (1:1)	3.57	11.16	3.99	266.87	2.97
PTO-C5-Li (2:1)	2.35	8.1	3.15	131.55	1.06
PTO-C5-Li (1:0)	2.1	6.49	2.93	106.26	0.68

[a]τ_3: ortho-positronium (o-Ps) pick-off lifetime; [b]I_3: o-Ps intensity; [c]R: the average radius of free volume holes; [d]V_f: the average free volume size; [e]f_v: the fraction of the free volume.

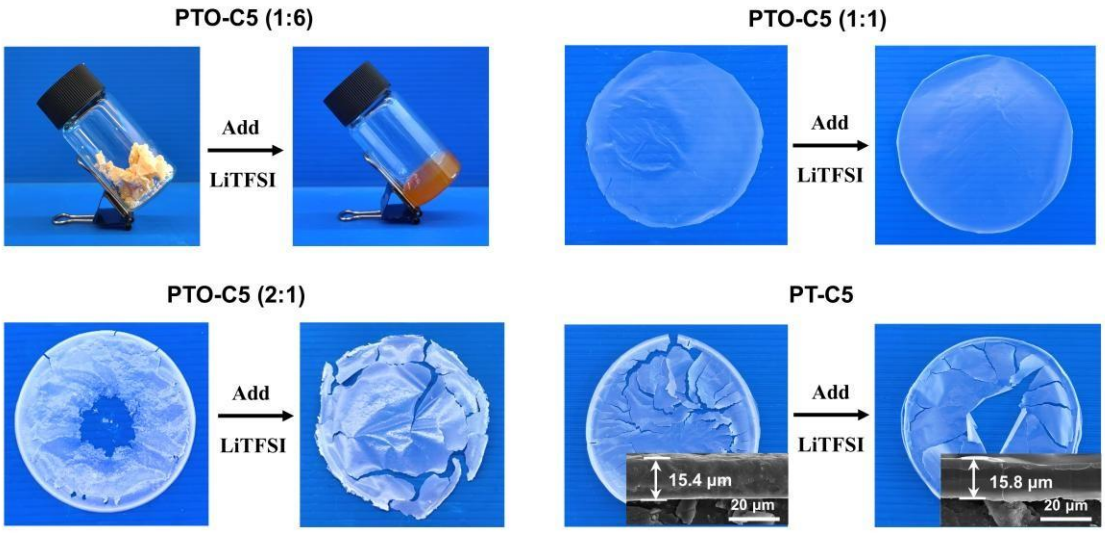

Fig. S17 Optic images of PTO-C5 (1:6), PTO-C5 (1:1), PTO-C5 (2:1) and PT-C5 before and after adding LiTFSI. The molar ratios of terephthalate to oxalate are fixed at 1:6, 1:1, 2:1 and 1:0, respectively.

a

Sample	Terephthalate : Oxalate	Molecular structure
POE-C5	0:1	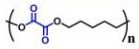
PTO-C5 (1:6)	1:6	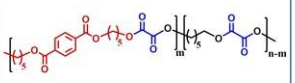
PTO-C5	1:3	
PTO-C5 (1:1)	1:1	
PTO-C5 (2:1)	2:1	
PT-C5	1:0	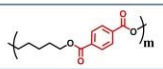

b

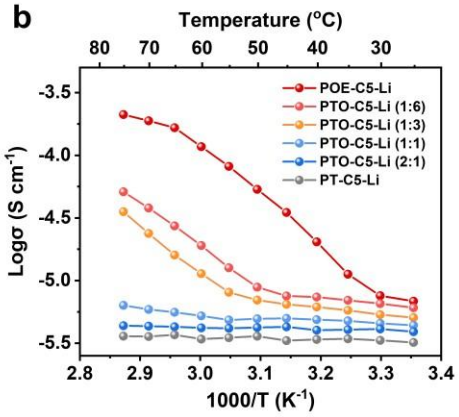

Fig. S18 (a) Molecular structures of polymers with different molar ratios of terephthalate to oxalate. (b) The Li^+-conductivity of POE-C5-Li, PTO-C5-Li (1:6), PTO-C5-Li, PTOC5-Li (1:1), PTO-C5-Li (2:1) and PT-C5-Li.

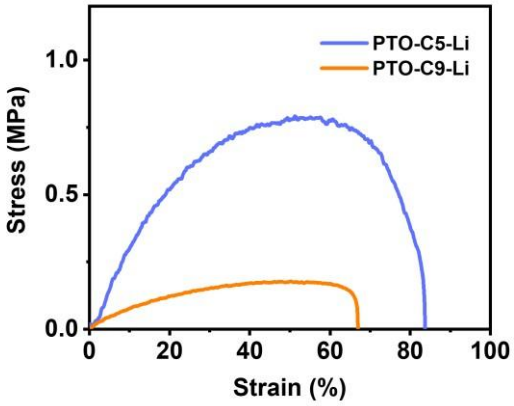

Fig. S19 Stress-strain curves of PTO-C5-Li and PTO-C9-Li.

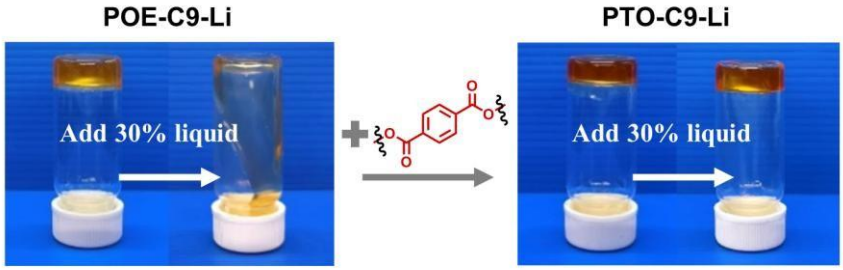

Fig. S20 Optic images of POE-C9-Li and PTO-C9-Li before and after adding 30 wt% liquid (L).

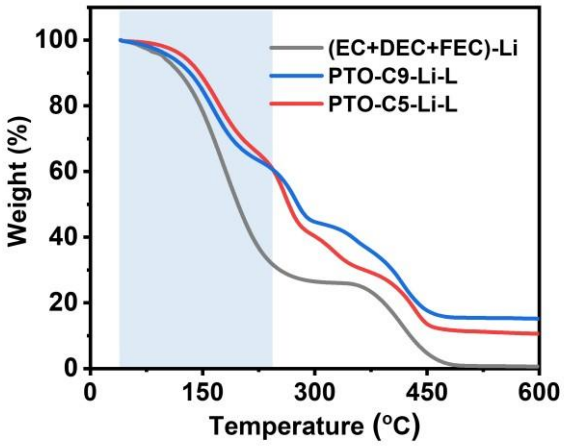

Fig. S21 Thermogravimetric analysis (TGA) curves of LiTFSI in EC+DEC+FEC (1:1:1 in weight ratio, 28.6 wt% LiTFSI), PTO-C9-Li-L and PTO-C5-Li-L. L represents liquid: 30 wt% of EC+DEC+FEC (1:1:1, weight ratio).

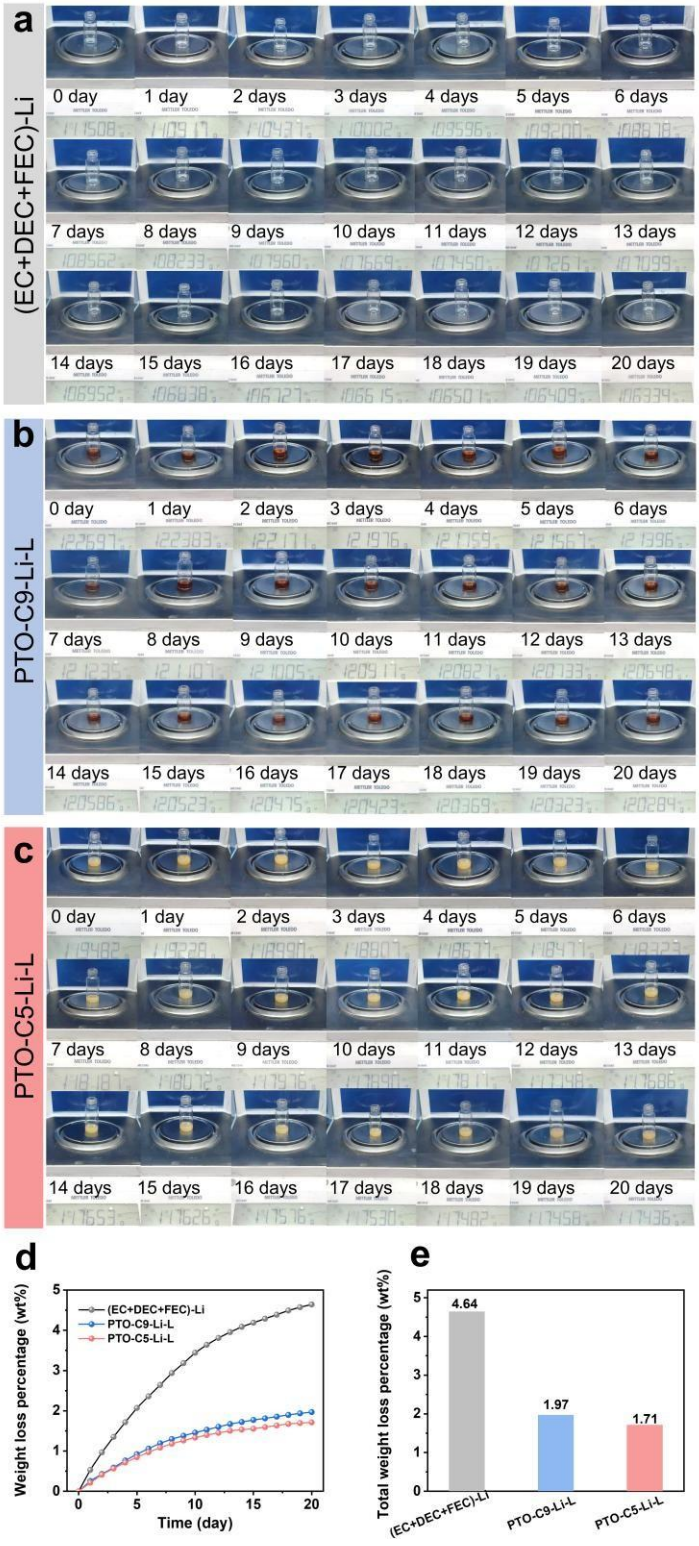

Fig. S22 Solvent volatility test of LiTFSI in EC+DEC+FEC (1:1:1 in weight ratio, 28.6 wt% LiTFSI), PTO-C9-Li-L and PTO-C5-Li-L for 20 days at room temperature. L represents liquid: 30 wt% of EC+DEC+FEC (1:1:1, weight ratio).

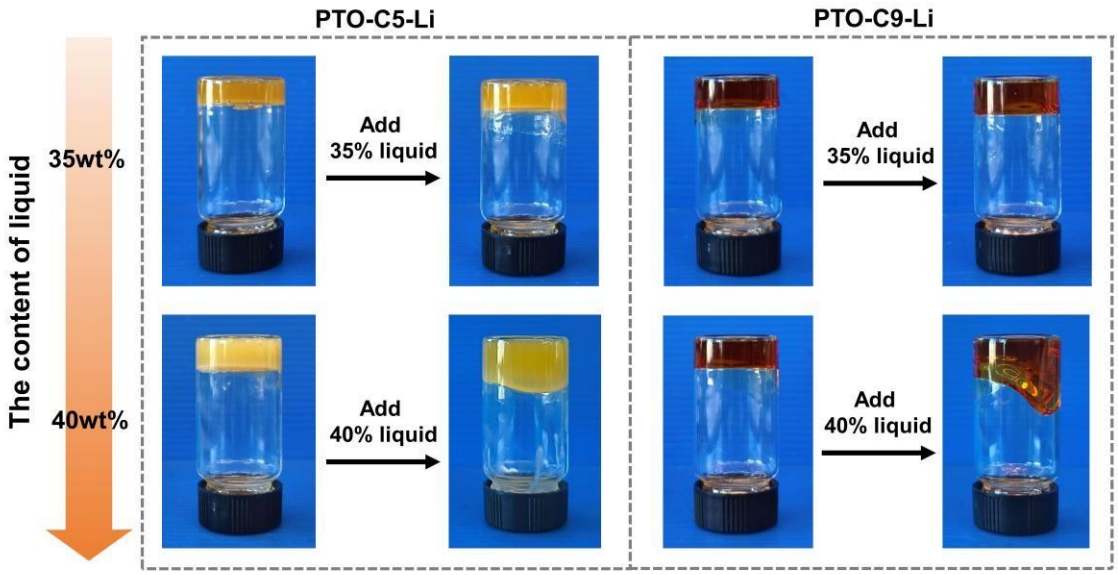

Fig. S23 Optic images of PTO-C5-Li and PTO-C9-Li before and after adding 35 wt% and 40 wt% liquid.

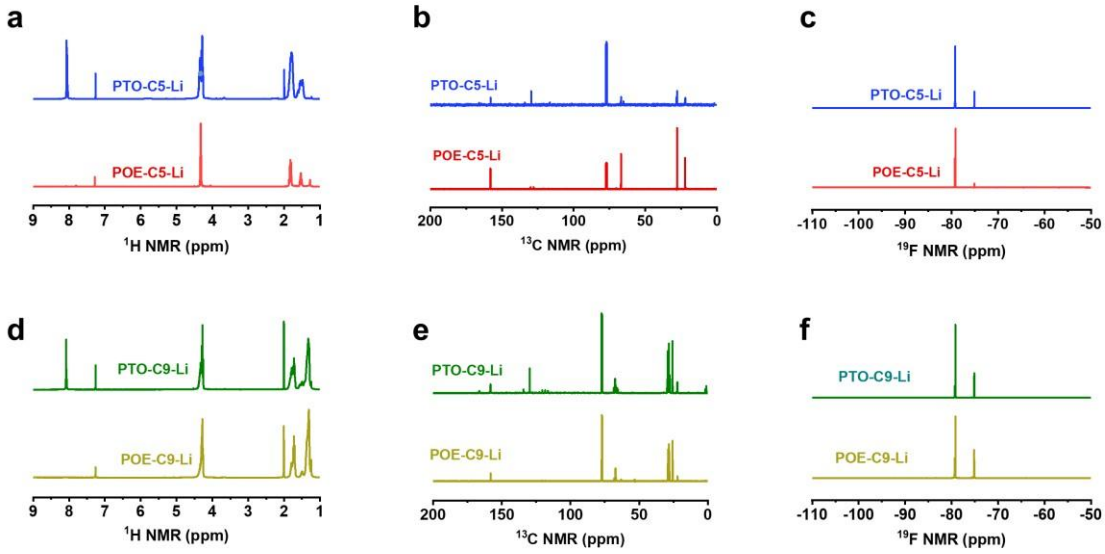

Fig. S24 (a) ^{1}H NMR, (b) ^{13}C NMR and (c) ^{19}F NMR spectra of POE-C5-Li and PTO-C5Li. (d) ^{1}H NMR, (e) ^{13}C NMR and (f) ^{19}F NMR spectra of POE-C9-Li and PTO-C9-Li (using $CDCl_3$ as solvent).

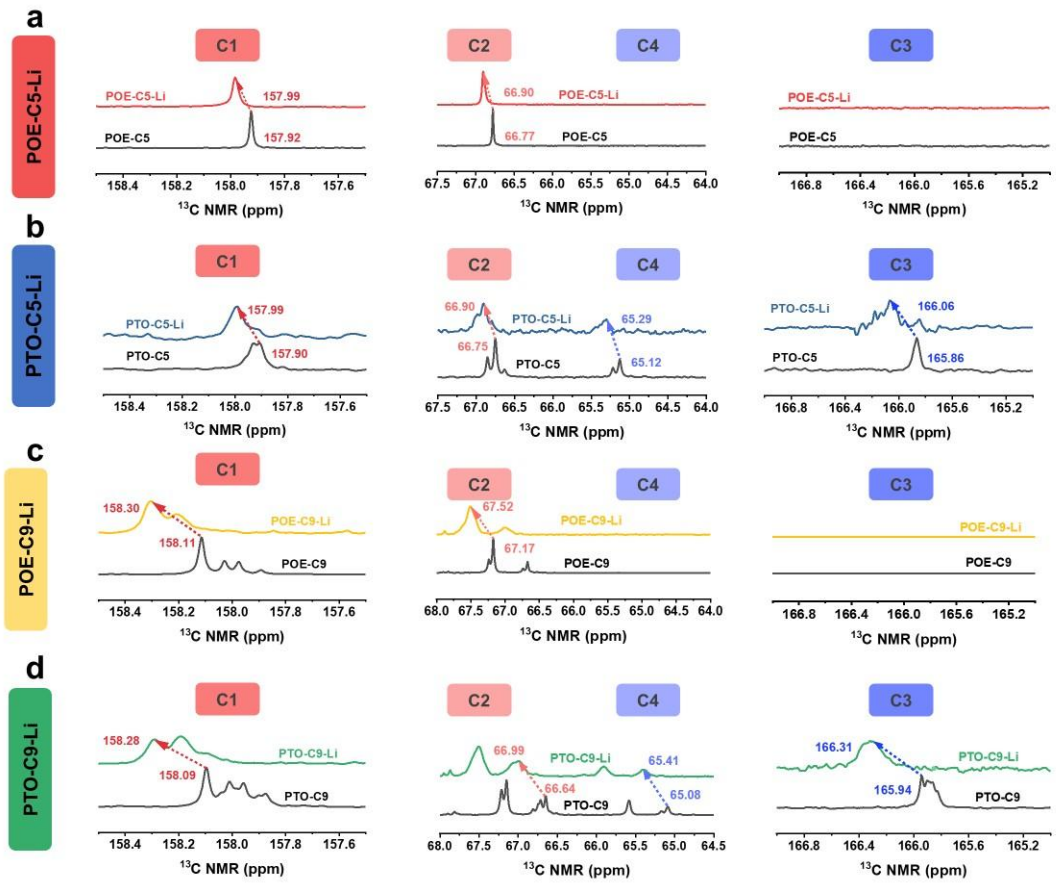

Fig. S25 The change of chemical shifts of carbonyl carbon (C=O) and alkoxy carbon (C–O) in POE and PTO-based polymers ($CDCl_3$ solution) with and without LiTFSI.

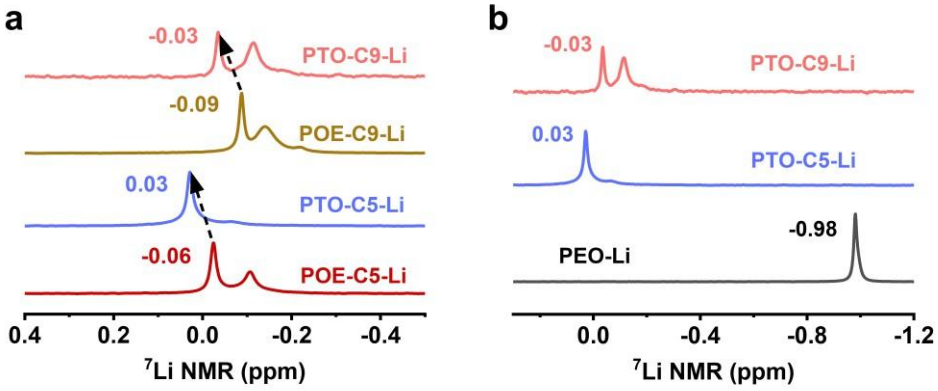

Fig. S26 ^{7}Li chemical shifts of (a) POE and PTO with LiTFSI and (b) PEO with LiTFSI in the weight ratio of polymer:LiTFSI = 2.5:1. The Li^+ signals in PTO-C5 and PTO-C9 electrolytes are located in a much lower field than that in PEO electrolytes, indicating a weaker coordination ability of PTO than PEO.

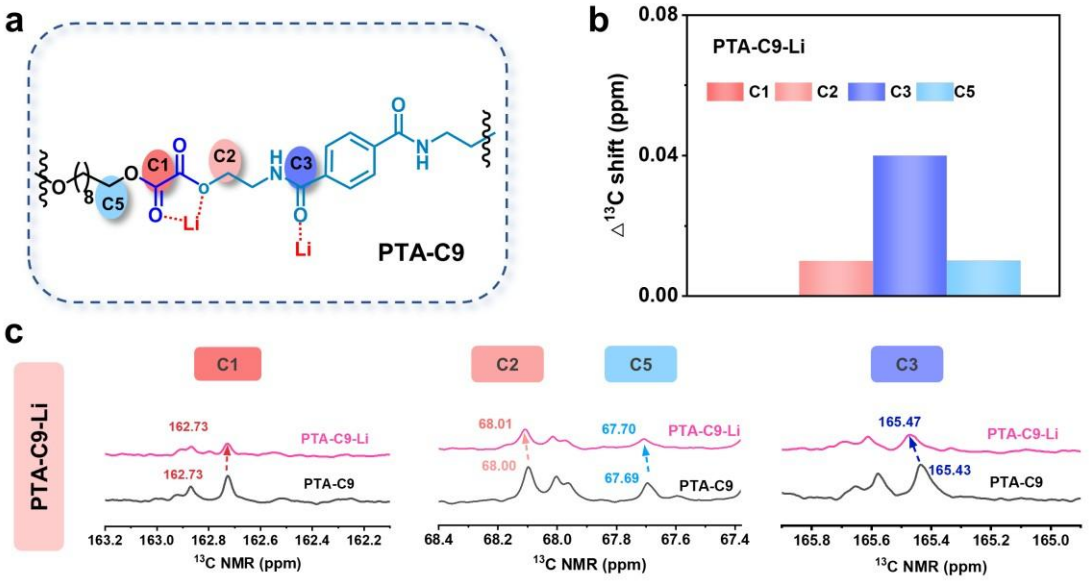

Fig. S27 (a) Labelled carbons of PTA-C9, (b) the chemical shift changes of ^{13}C NMR spectra of labelled carbonyl carbon (C=O) and alkoxy carbon (C–O) before and after adding LiTFSI, and (c) the corresponding chemical shifts of ^{13}C NMR.

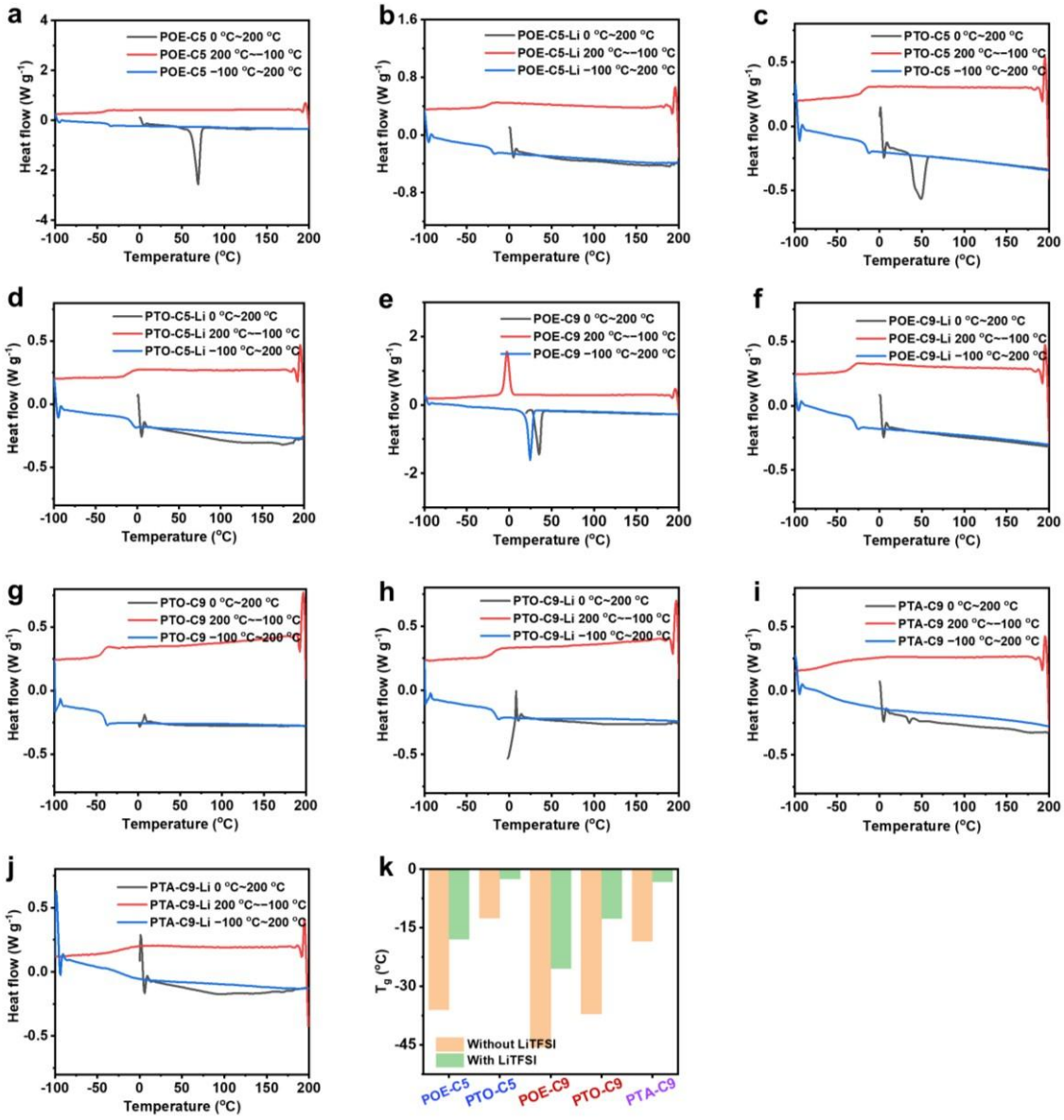

Fig. S28 (a-j) Differential scanning calorimetry (DSC) curves of POE, PTO and PTAbased polymers without and with LiTFSI. (k) Comparison of glass transition temperatures (T_g).

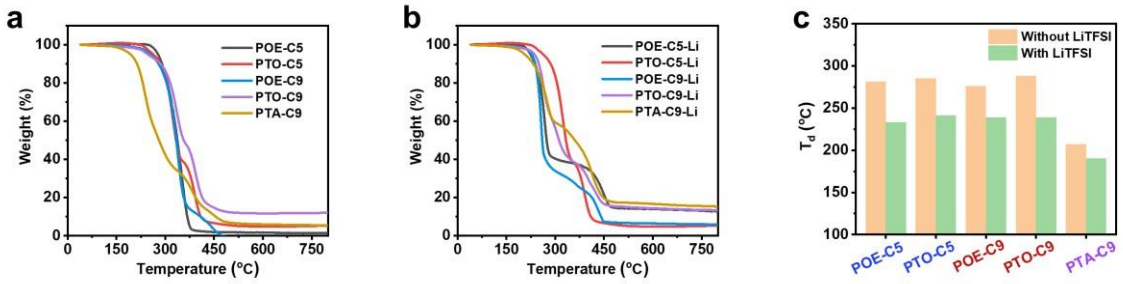

Fig. S29 Thermogravimetric analysis (TGA) curves of POE, PTO and PTA-based polymers (a) without LiTFSI, (b) with LiTFSI. (c) Comparison of decomposition onset temperatures (T_d) of polymers with and without LiTFSI.

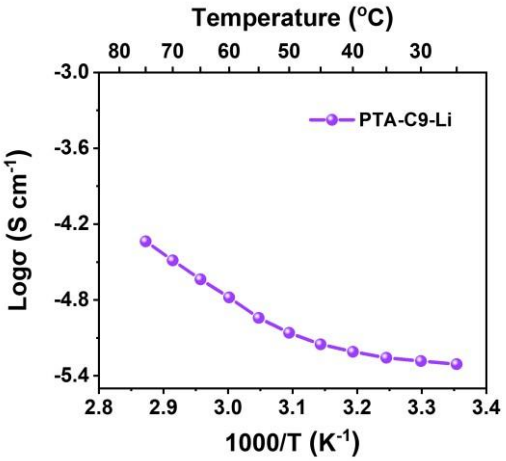

Fig. S30 The Li^+-conductivity of dry PTA-C9-Li SPEs in the weight ratio of polymer:LiTFSI = 2.5:1.

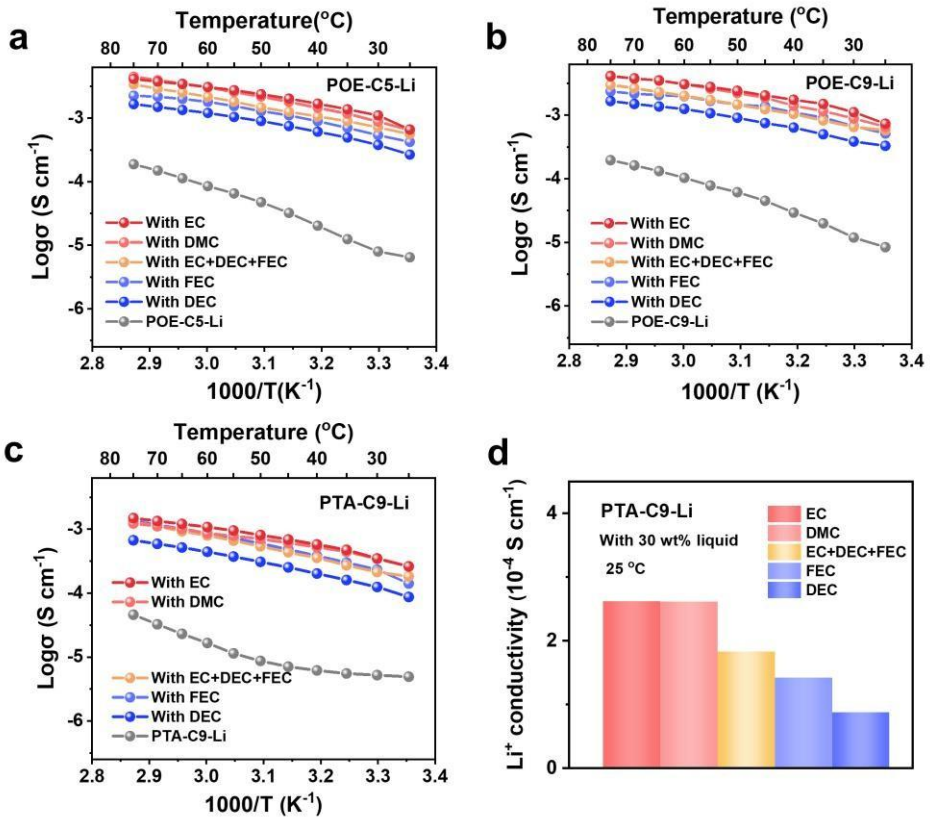

Fig. S31 The Li^+-conductivity of (a) POE-C5-Li, (b) POE-C9-Li, (c) PTA-C9-Li with and without 30 wt% liquid at 25 °C–75 °C. The weight ratio of the mixture of EC+DEC+FEC is 1:1:1. (d) Li^+-conductivity of PTA-C9-Li containing 30 wt% different liquid electrolytes at 25 °C.

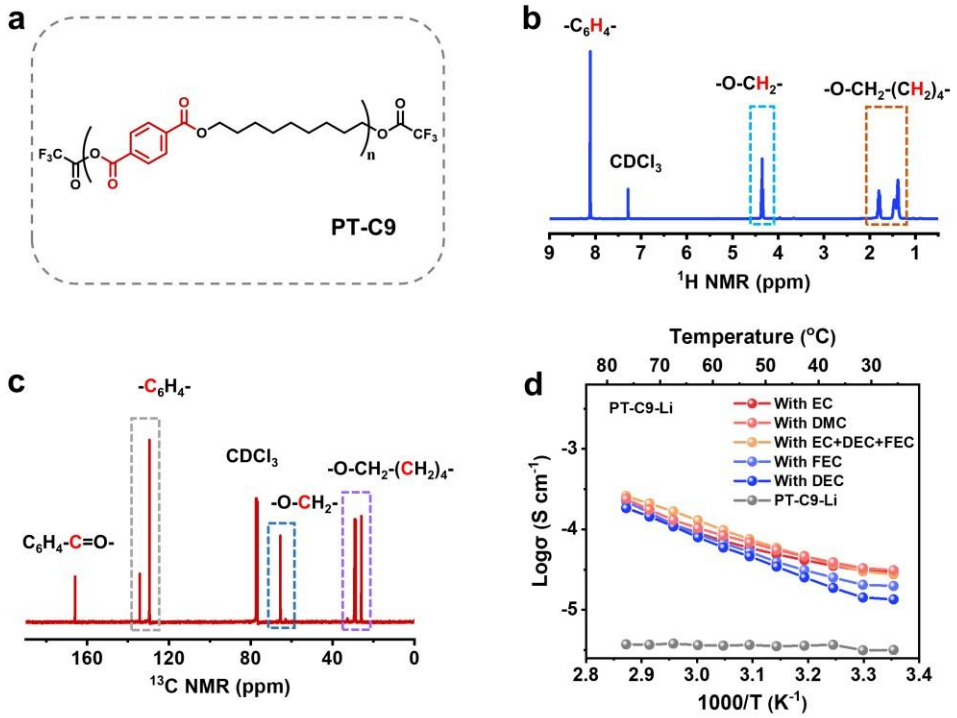

Fig. S32 (a) Molecular structure of PT-C9. (b) ^{1}H NMR and (c) ^{13}C NMR spectra of PTC9. (d) Li^{+}-conductivity of PT-C9 with and without 30 wt% liquid at 25 °C–75 °C. The weight ratio of the mixture of EC+DEC+FEC is 1:1:1.

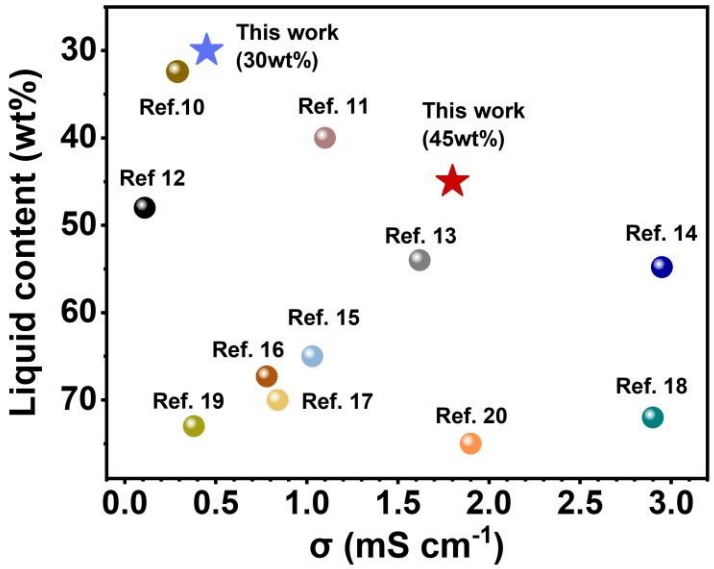

Fig. S33 Comparison of the liquid contents and ionic conductivities between PTO-C9-LiL (30 wt% or 45 wt% of EC) and reported QSSEs.

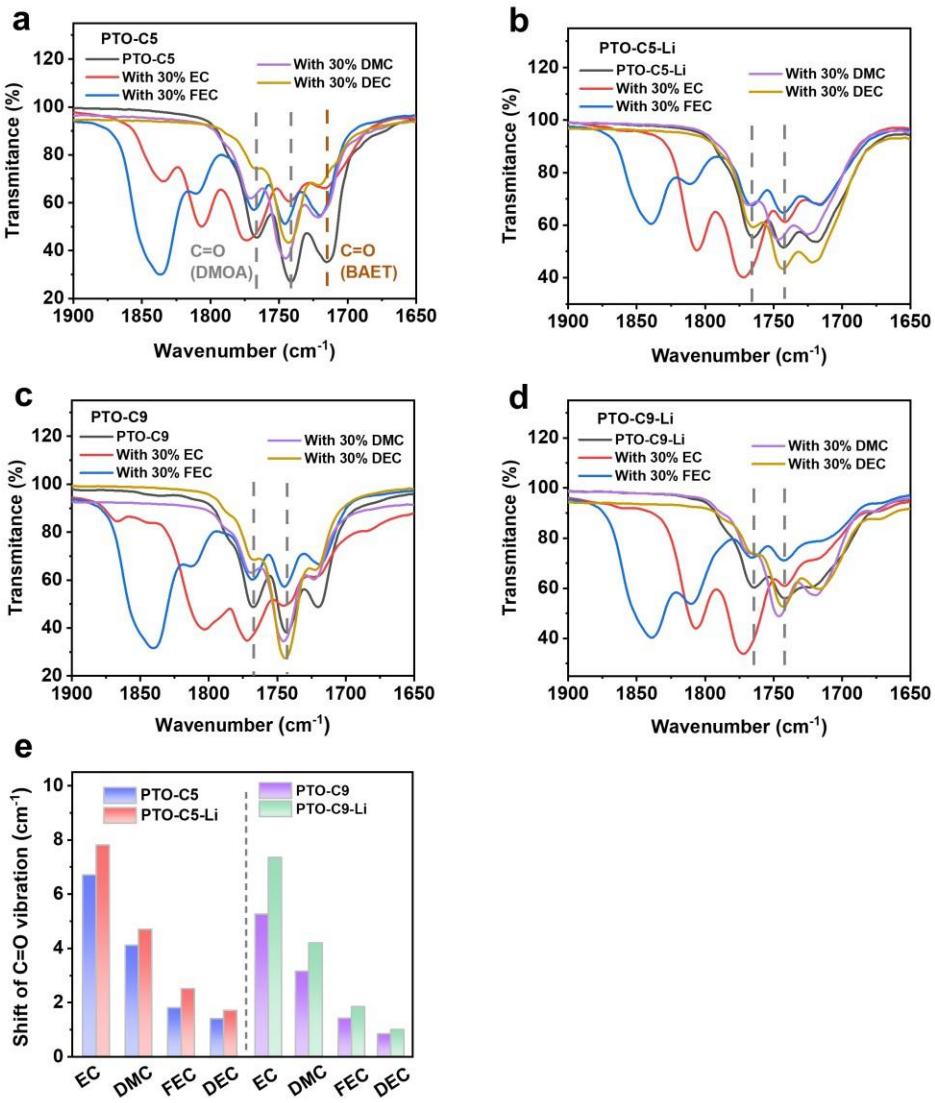

Fig. S34 Fourier Transform Infrared Spectroscopy (FT-IR) spectra of (a, b) PTO-C5 and (c, d) PTO-C9 in the presence of different solvents and with and without LiTFSI. (e) C=O vibration shifts of PTO-C5 and PTO-C9 in the FT-IR spectra (liquids: 30 wt%, with and without LiTFSI).

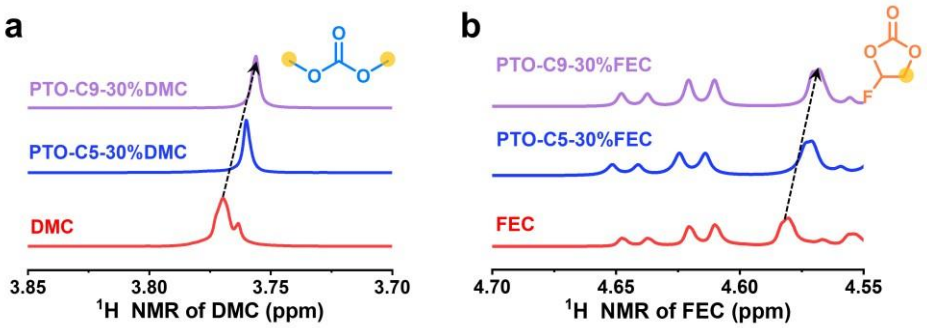

Fig. S35 ^{1}H NMR chemical shift of (a) DMC and (b) FEC in the presence of different polymers and without LiTFSI. In these ^{1}H NMR spectra, the H atoms corresponding to the peaks are labelled using colorful circular spots.

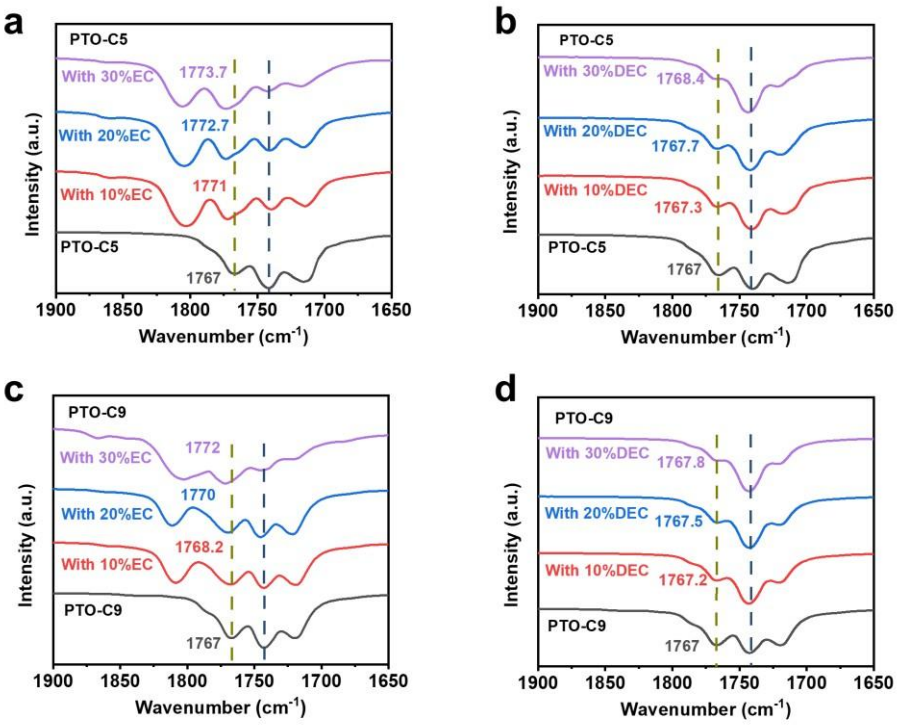

Fig. S36 FT-IR spectra of (a, b) PTO-C5 and (c, d) PTO-C9 with and without 10 wt%, 20 wt% and 30 wt% EC or DEC.

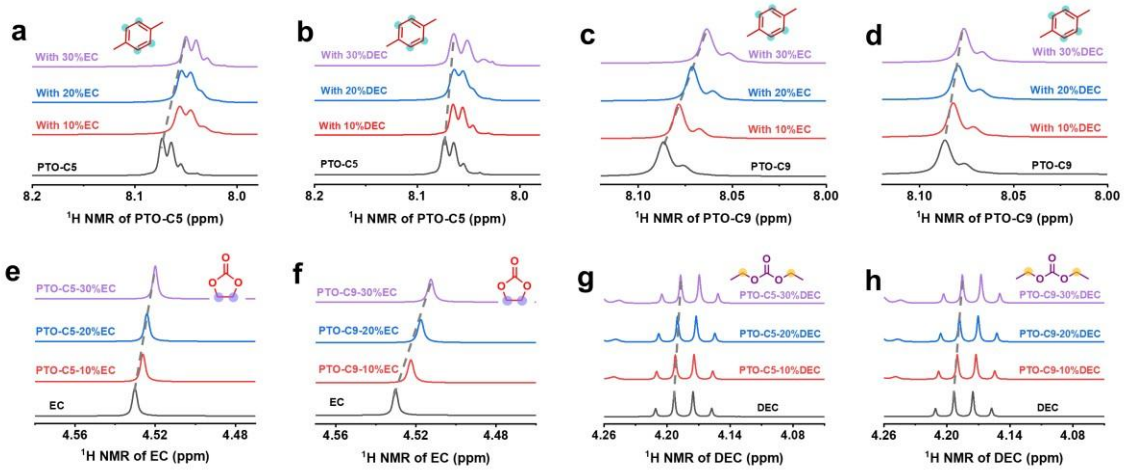

Fig. S37 ^{1}H NMR spectra of (a, b) PTO-C5 and (c, d) PTO-C9 with and without 10 wt%, 20 wt%, 30 wt% EC or DEC. ^{1}H NMR spectra of (e, f) EC and (g, h) DEC in PTO-C5 or PTO-C9 with different liquid content. In these ^{1}H NMR spectra, the H atoms corresponding to the peaks are labelled using colorful circular spots.

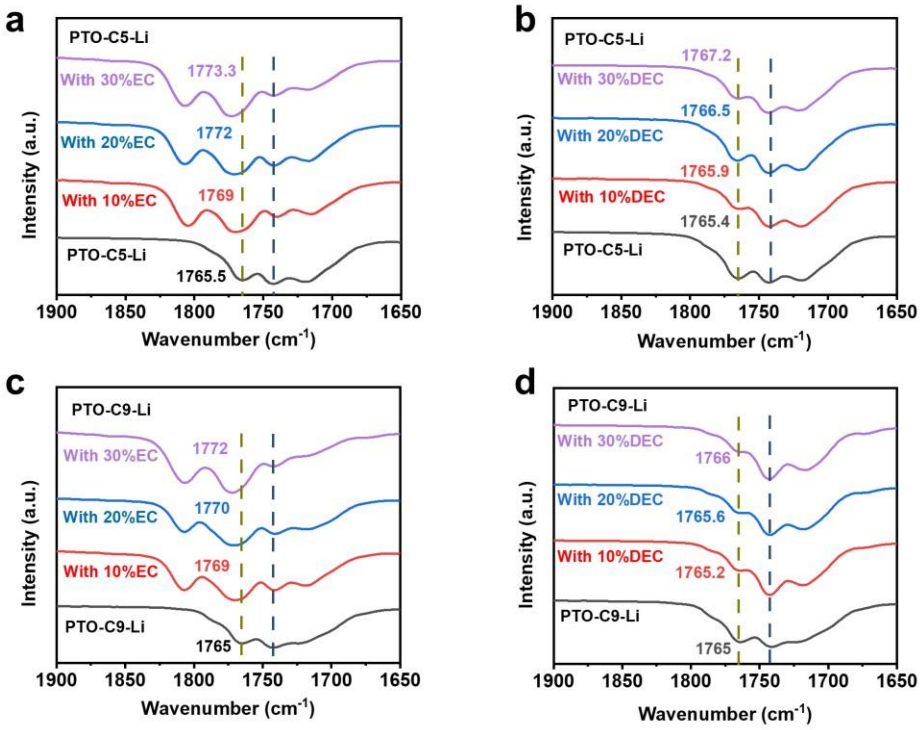

Fig. S38 FT-IR spectra of (a, b) PTO-C5-Li and (c, d) PTO-C9-Li with and without 10 wt%, 20 wt% and 30 wt% EC or DEC.

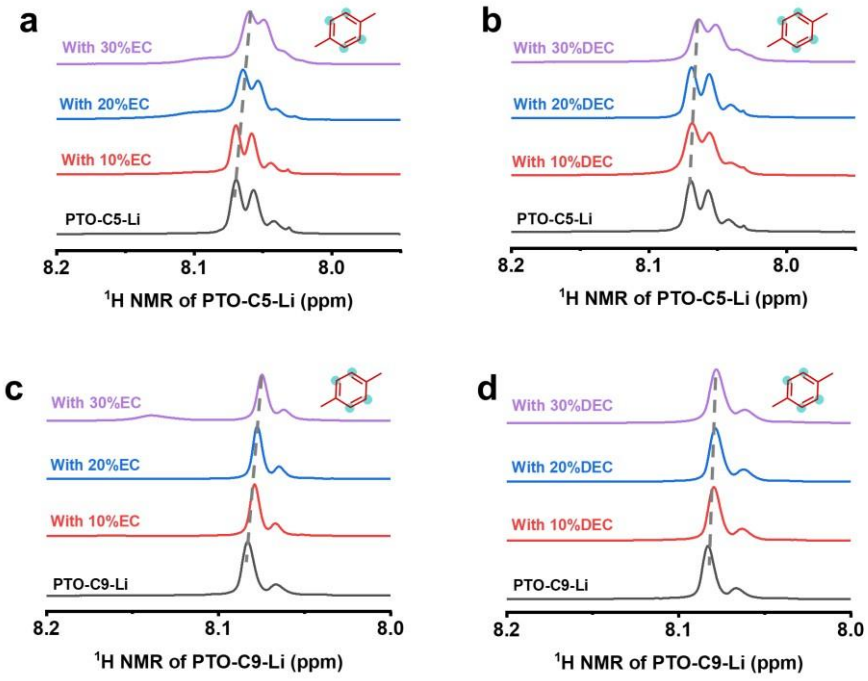

Fig. S39 ^{1}H NMR spectra of (a, b) PTO-C5-Li and (c, d) PTO-C9-Li with and without 10 wt%, 20 wt% 30 wt% EC or DEC. In these ^{1}H NMR spectra, the H atoms corresponding to the peaks are labelled using colorful circular spots.

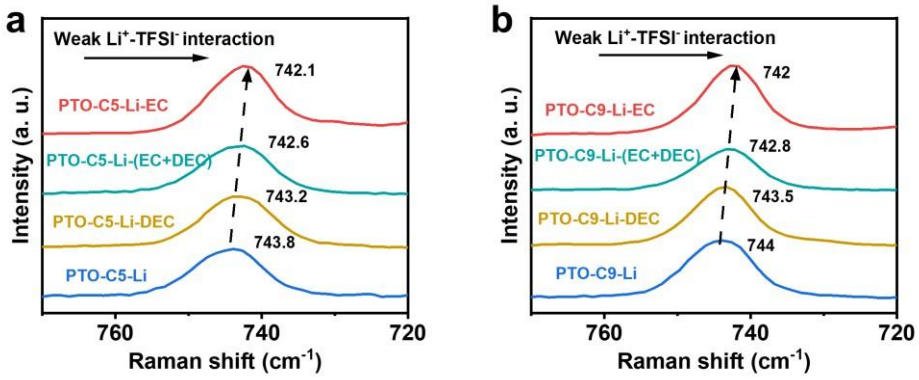

Fig. S40 Raman spectra of $TFSI^{-}$ vibration of (a) PTO-C5-Li, (b) PTO-C9-Li without and with 30 wt% EC, EC+DEC (EC:DEC = 2:1, weight ratio), or DEC.

Table S4. Components and the corresponding numbers for the solvation structure simulation of PTO-C5-Li with 30 wt% of EC, DEC, or EC+DEC (2:1, weight ratio) by molecular dynamics (MD).

System	Number of each component				
	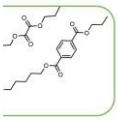		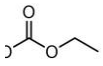	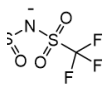	Li^+
[a]PTO-C5-Li-EC	[b]58	342	---	100	100
PTO-C5-Li-DEC	58	---	255	100	100
PTO-C5-Li-(EC+DEC)	58	228	85	100	100

[a] PTO-C5:

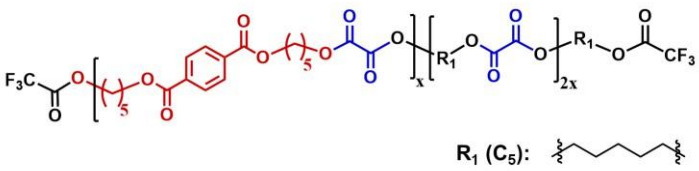

[b] 58 means that 58 numbers of [terephthalate–$(CH_2)_5$–oxalate] segments and 58 numbers of [oxalate–$(CH_2)_5$–oxalate] segments, representing 58 numbers of OOTO1-1.

In PTO-C5, the molar ratio of terephthalate to oxalate is fixed at 1:3. The repeating units of PTO-C5 contain [$(CH_2)_5$–terephthalate–$(CH_2)_5$–oxalate] and [$(CH_2)_5$–oxalate] in the molar ratio of 1:2. Owing to the excessive length of the PTO repeating units, the conformation modeling is difficult to convergence. Accordingly, the repeating units were divided into two representative segments of [terephthalate–$(CH_2)_5$–oxalate] and [oxalate–$(CH_2)_5$–oxalate] in the molar ratio of 1:1 for simulation, defined as OOTO1-1. The molar ratios of EC:(OOTO1-1):LiTFSI = 3.4:0.6:1, DEC:(OOTO1-1):LiTFSI = 2.6:0.6:1 and (EC+DEC): (OOTO1-1):LiTFSI = 3.1:0.6:1 correspond to the real molar ratios in PTObased QSSEs with 30 wt% solvent.

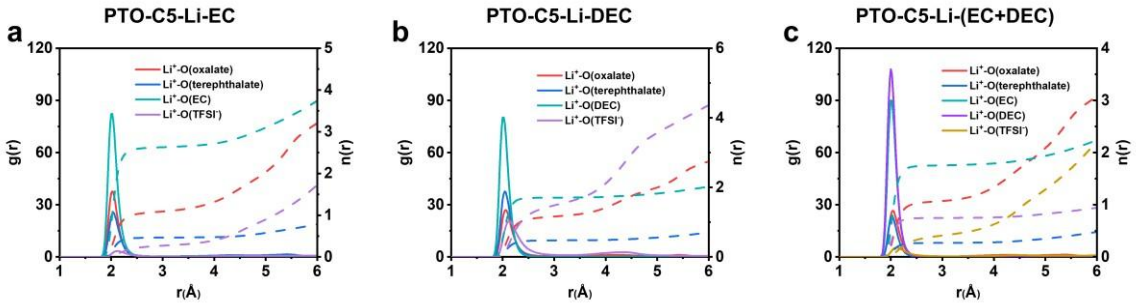

Fig. S41 Radial distribution function (g(r)) and coordination numbers (n(r)) of PTO-C5-Li with 30 wt% (a) EC, (b) DEC and (c) EC+DEC (2:1).

Table S5. The coordination numbers of the primary solvation sheath of Li^+ in PTO-C5-LiEC, PTO-C5-Li-DEC and PTO-C5-Li-(EC+DEC).

System	Coordination number				
	Li-O (C=O of **PTO-C5**)		Li-O (C=O of **EC**)	Li-O (C=O of **DEC**)	Li-O (S=O of **$TFSI^-$**)
	Li-O (C=O of **oxalate**)	Li-O (C=O of **terephthalate**)			
PTO-C5-Li-EC	1.1	0.5	2.6	---	0.3
PTO-C5-Li-DEC	1.2	0.5	---	1.7	1.6
PTO-C5-Li-(EC+DEC)	1.1	0.3	1.8	0.8	0.4

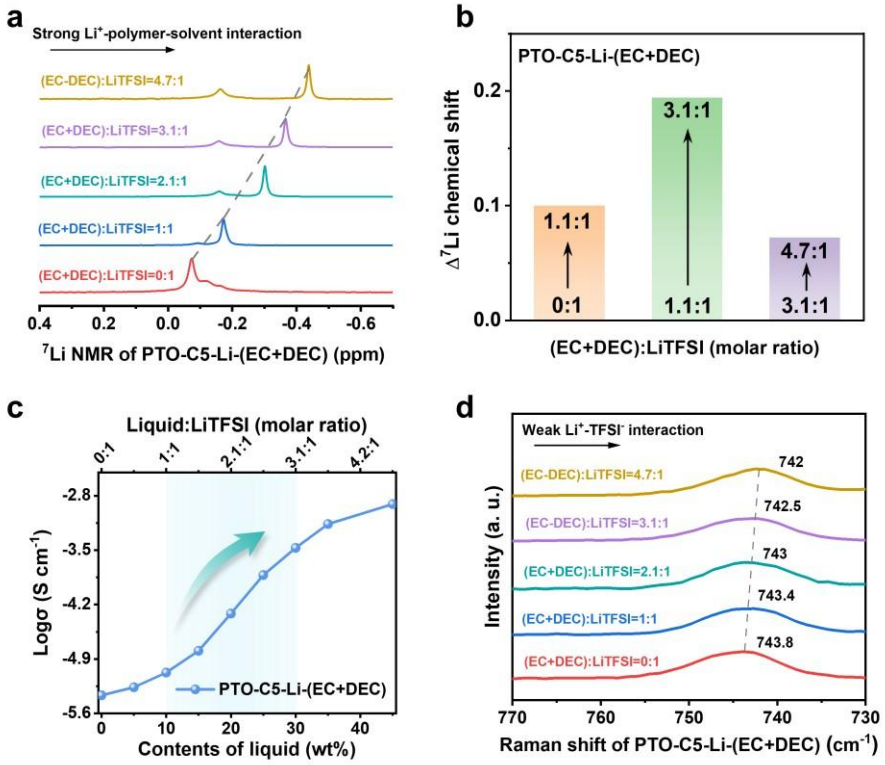

Fig. S42 (a) ^{7}Li NMR of PTO-C5-Li-(EC+DEC) with different solvent-to-salt ratio ((EC+DEC):LiTFSI = 0:1 to 4.7:1). (b) Collected Δ^{7}Li chemical shift of PTO-C5(EC+DEC) with (EC+DEC):LiTFSI = 0:1−1:1, (EC+DEC):LiTFSI = 1:1−3.1:1 and (EC+DEC):LiTFSI = 3.1:1−4.7:1. (c) Li^{+}-conductivity of PTO-C5-Li-(EC+DEC) with different solvent contents. (d) Raman spectra of $TFSI^{-}$ vibration of PTO-C5-Li-(EC+DEC) with different solvent-to-salt ratio ((EC+DEC):LiTFSI = 0:1 to 4.7:1).

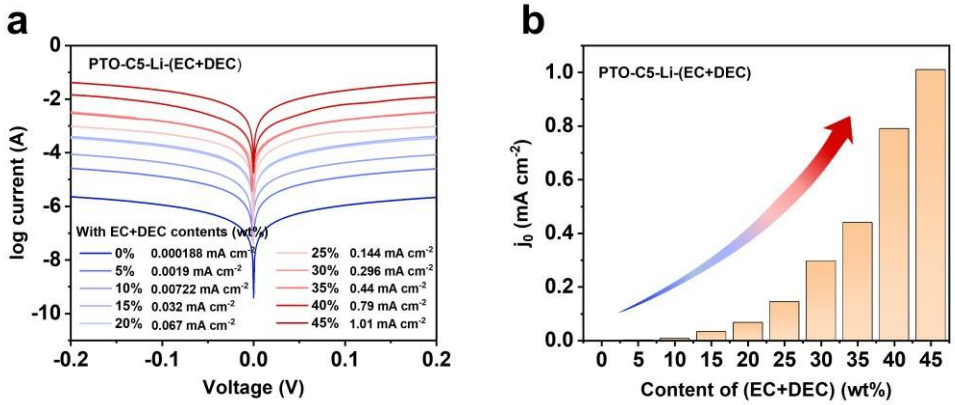

Fig. S43 Tafel plots of PTO-C5-Li-(EC+DEC) with different contents of liquids.

Table S6 Components and the corresponding numbers for the solvation structure simulation of PTO-C5-Li-(EC+DEC) with 10 wt%, 30 wt%, and 45 wt% of (EC+DEC) (2:1, weight ratio) by molecular dynamics (MD).

[a]PTO-C5-Li-(EC+DEC)	Number of each component				
	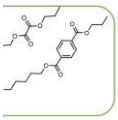		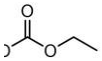	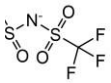	Li^+
(EC+DEC):LiTFSI=1:1	[b]87	76	28	100	100
(EC+DEC):LiTFSI=3.1:1	58	228	85	100	100
(EC+DEC):LiTFSI=4.7:1	37	342	128	100	100

[a] PTO-C5:

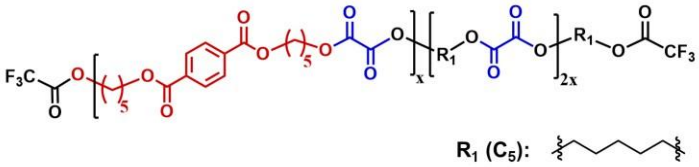

[b] 87 means that 87 numbers of [terephthalate–$(CH_2)_5$–oxalate] segments and 87 numbers of [oxalate–$(CH_2)_5$–oxalate] segments, representing 87 numbers of OOTO1-1.

In PTO-C5, the molar ratio of terephthalate to oxalate is fixed at 1:3. The repeating units of PTO-C5 contain [$(CH_2)_5$–terephthalate–$(CH_2)_5$–oxalate] and [$(CH_2)_5$–oxalate] in the molar ratio of 1:2. Owing to the excessive length of the PTO repeating units, the conformation modeling is difficult to convergence. Accordingly, the repeating units were divided into two representative segments of [terephthalate–$(CH_2)_5$–oxalate] and [oxalate–$(CH_2)_5$–oxalate] in the molar ratio of 1:1 for simulation, defined as OOTO1-1. The EC+DEC content increases from 10 wt% to 30 wt% and then 45 wt%, corresponding to the (EC+DEC):(OOTO1-1):LiTFSI molar ratio rising from 1:0.9:1 to 3.1:0.6:1 and then 4.7:0.4:1.

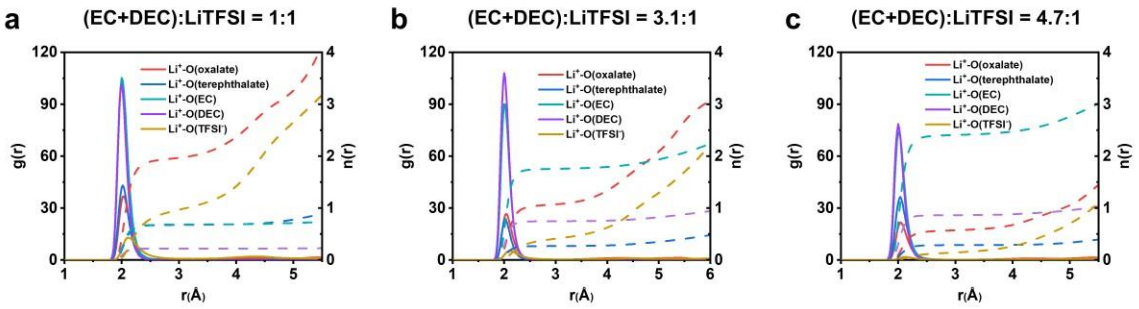

Fig. S44 Radial distribution function (g(r)) and coordination numbers (n(r)) of PTO-C5Li-(EC+DEC) with different solvent contents of (a) (EC+DEC):LiTFSI = 1:1, (b) (EC+DEC):LiTFSI = 3.1:1 and (c) (EC+DEC):LiTFSI = 4.7:1.

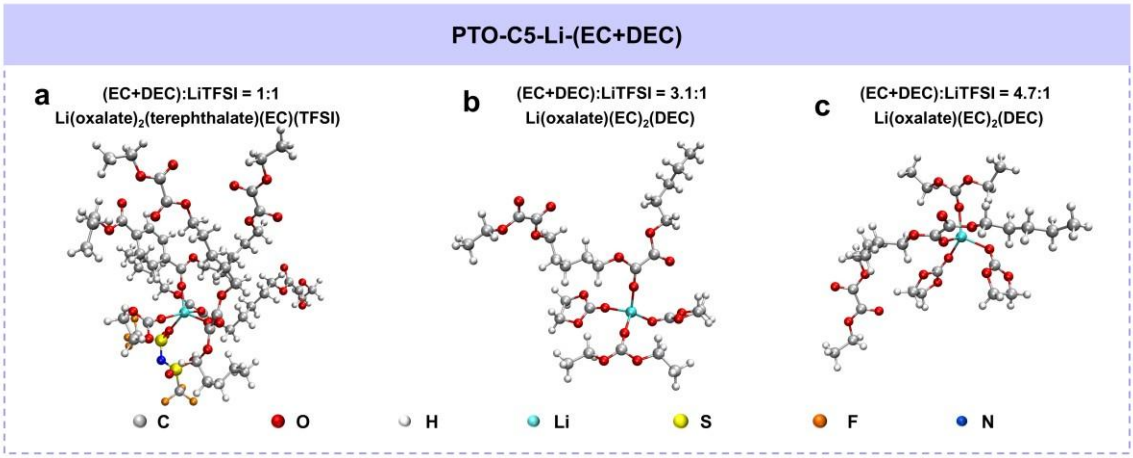

Fig. S45 The representative Li^+ solvation structures of PTO-C5-Li-(EC+DEC) with different solvent contents of (a) (EC+DEC):LiTFSI = 1:1, (b) (EC+DEC):LiTFSI = 3.1:1 and (c) (EC+DEC):LiTFSI = 4.7:1 simulated by MD.

Table S7. The coordination numbers of the primary solvation sheath of Li^+ in PTO-C5-Li(EC+DEC) with different solvent contents.

PTO-C5-Li-(EC+DEC)	Coordination number				
	Li-O (C=O of **PTO-C5**)		Li-O (C=O of **EC**)	Li-O (C=O of **DEC**)	Li-O (S=O of **TFSI**$^-$)
	Li-O (C=O of **oxalate**)	Li-O (C=O of **terephthalate**)			
(EC+DEC):LiTFSI = 1:1	2	0.7	0.7	0.2	1
(EC+DEC):LiTFSI = 3.1:1	1.1	0.3	1.8	0.8	0.4
(EC+DEC):LiTFSI = 4.7:1	0.6	0.3	2.4	0.9	0.2

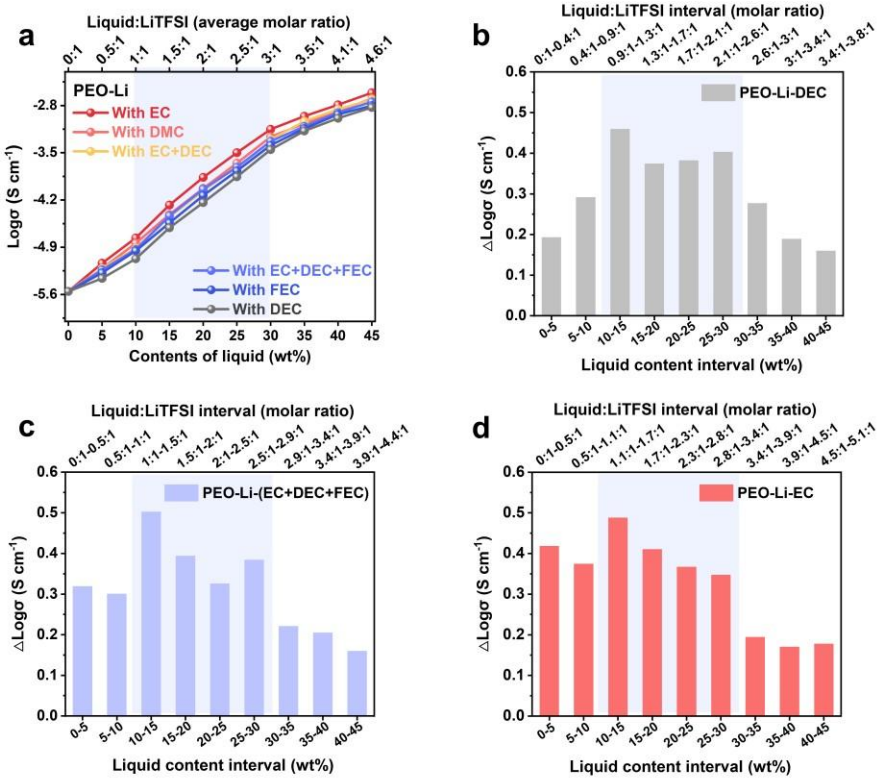

Fig. S46 (a) Li^+-conductivity of PEO-based QSSEs with different contents of liquids. The liquid:LiTFSI molar ratio (top X-axis) represents the average molar ratio from all QSSE samples at each liquid content. The corresponding Li^+-conductivity increments in different liquid content interval with (b) DEC, (c) EC+DEC+FEC, and (d) EC.

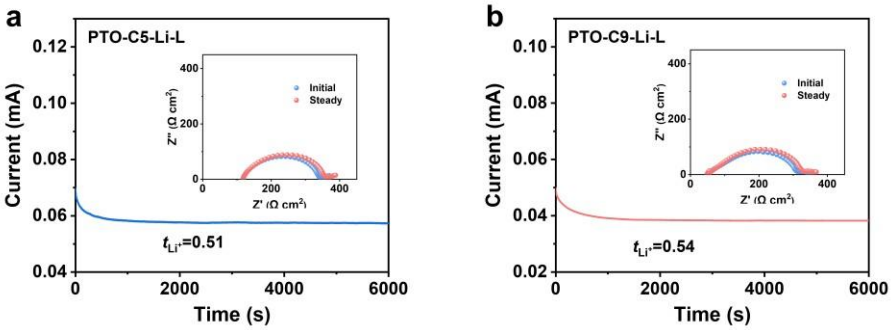

Fig. S47 Current-time profile following a polarization of 10 mV for Li//Li cell with PTOC5-Li-L, (b) PTO-C9-Li-L. The inset displays the Nyquist profiles of electrochemical impedance curves before and after polarization. L represents liquid: 30 wt% of EC+DEC+FEC (1:1:1, weight ratio).

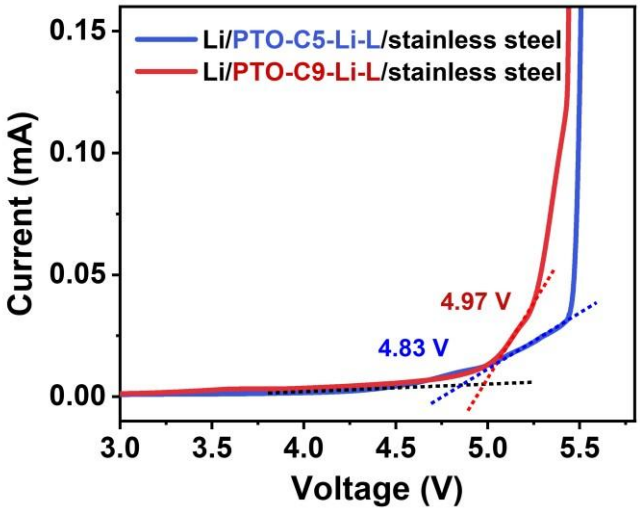

Fig. S48 The linear sweep voltammetry curves of PTO-C5-Li-L and PTO-C9-Li-L in Li//stainless steel cells from open circuit voltage (OCV) to 5.5 V. L represents liquid: 30 wt% of EC+DEC+FEC (1:1:1, weight ratio).

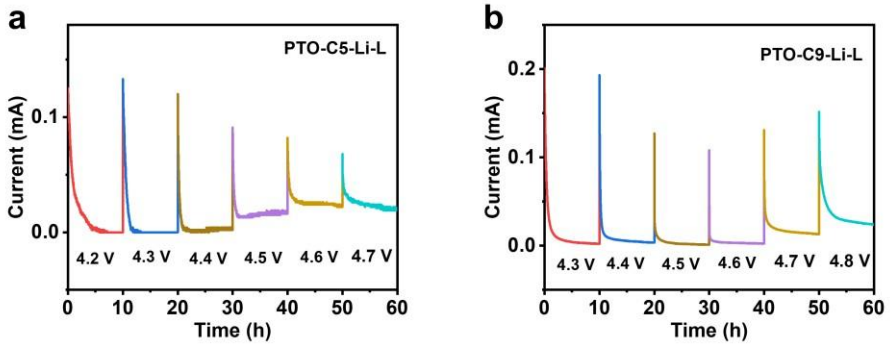

Fig. S49 The electrochemical floating test of Li//NCM85 cells using (a) PTO-C5-Li-L and (b) PTO-C9-Li-L. L represents liquid: 30 wt% of EC+DEC+FEC (1:1:1, weight ratio).

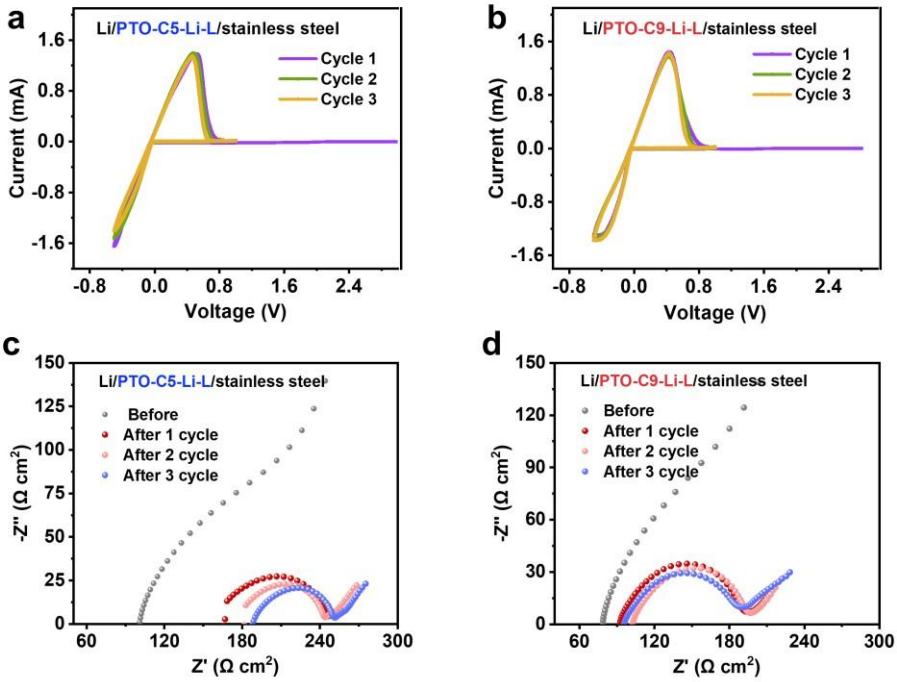

Fig. S50 The cyclic voltammetry curves of (a) PTO-C5-Li-L and (b) PTO-C9-Li-L in Li//stainless steel cells scanning from OCV to −0.5 V and then back to 1.0 V (25 ^{o}C). Subsequent cycles were scanned from 1.0 V to −0.5 V and then back to 1.0 V (25 ^{o}C). The scanning rate maintains at 0.2 mV s^{-1} at 25 ^{o}C. Corresponding impedance curves of Li//stainless steel cells using (c) PTO-C5-Li-L, (d) PTO-C9-Li-L. L represents liquid: 30 wt% of EC+DEC+FEC (1:1:1, weight ratio).

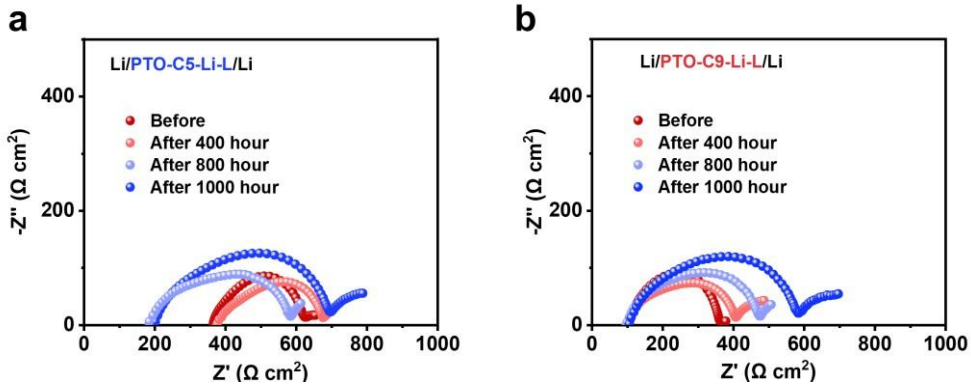

Fig. S51 The impedance curves of Li//Li cells using (a) PTO-C5-Li-L and (b) PTO-C9-LiL. L represents liquid: 30 wt% of EC+DEC+FEC (1:1:1, weight ratio).

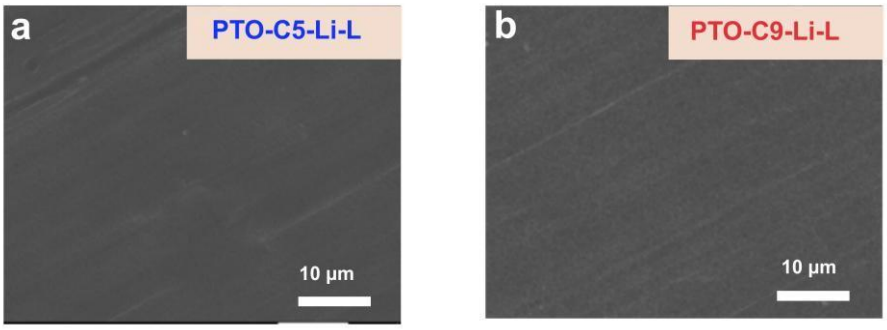

Fig. S52 SEM images of Li-foil surface after cycling 200 hours in Li//Li cells with (a) PTO-C5-Li-L and (b) PTO-C9-Li-L. L represents liquid: 30 wt% of EC+DEC+FEC (1:1:1, weight ratio).

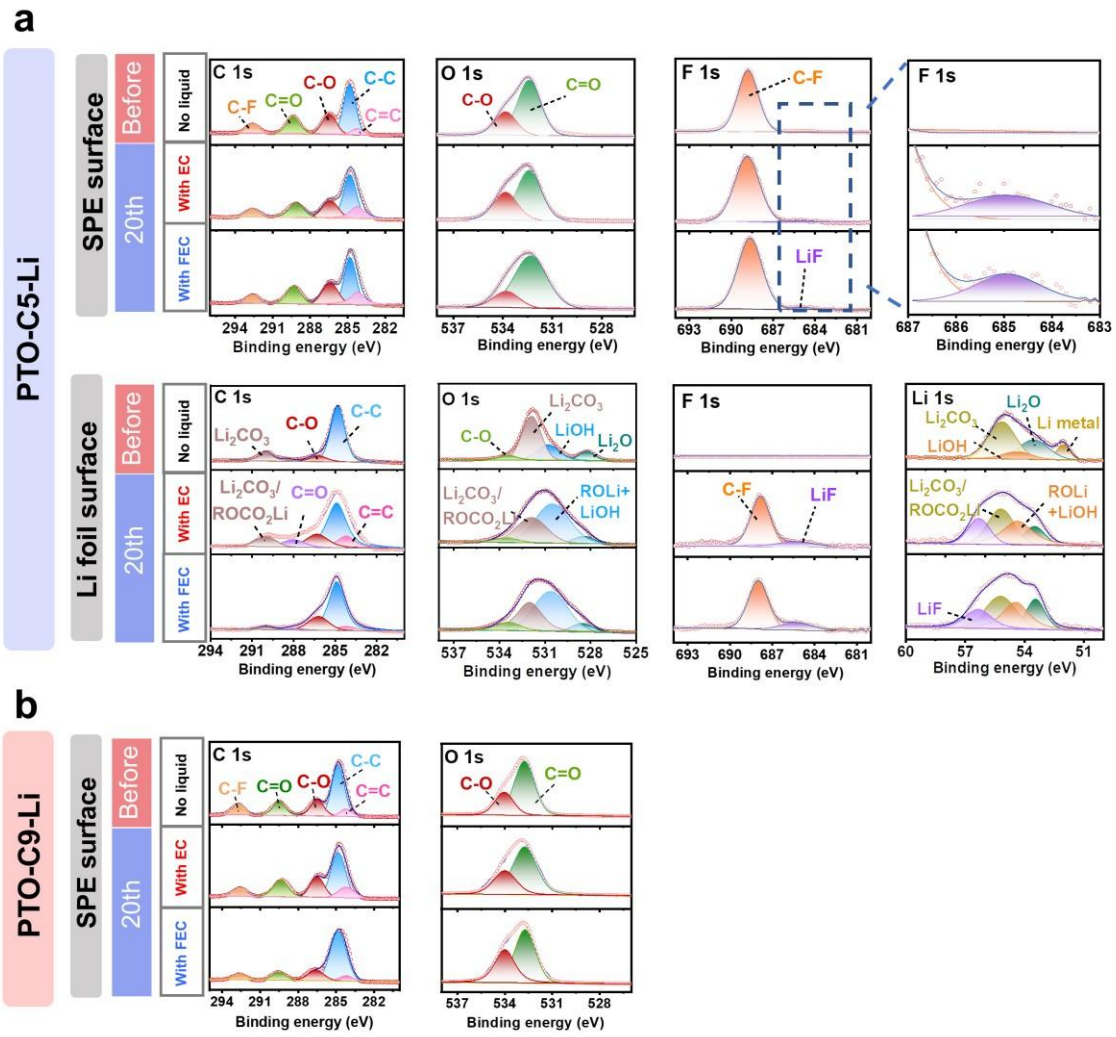

Fig. S53 (a) XPS spectra of PTO-C5-Li membranes without solvent and Li-foil before cycling, as well as PTO-C5-Li membranes with 30 wt% EC or 30 wt% FEC and the coupled Li-foil after cycling 20 cycles. (b) XPS spectra of PTO-C9-Li membranes without solvent before cycling, and with EC or FEC after cycling 20 cycles.

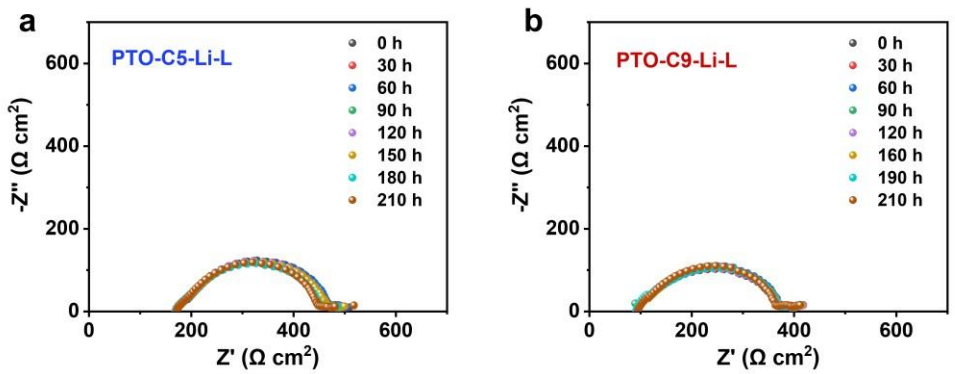

Fig. S54 The EIS plots of Li//Li cells with (a) PTO-C5-Li-L and (b) PTO-C9-Li-L for the distribution of relaxation times (DRT) analysis.

Table S8. Comparison of the electrochemical window and cell cycling stability between PTO-C9-Li-L and reported QSSEs.

QSSEs	Liquid in QSSEs	Liquid content (wt%)	Oxidation potential (V) (Floating test)	Cell	Cycling condition and capacity retention	Ref.
[a]FEC TFOA gel	FEC	~32.4	5	Li//NCM811	0.2C cycling, 81% after 140 cycles	10
[b]PCEE	Succinonitrile	~40	4.75 (4.6 V)	Li//NCM83	2C cycling, 88% after 100 cycles	11
[c]PP-LTPO CSE	Polyethylene glycol dimethyl ether (Mn ≈ 250)	48	4.7	Li//LCO	0.2C cycling, 85% after 100 cycles	12
[d]P(AEEO) based QSSE	EC+DEC+FEC	54	/ (>5 V)	Li//NCM85	1C cycling, 81.4% after 500 cycles	13
[e]Fluorinated quasisolid polymer electrolyte	Methyl 3,3,3trifluoropropanoate + FEC	54.8	5.2 (>5 V)	Li//NCM811	0.3C cycling, 86% after 200 cycles	14
[f]35TFMA-0.5LF0.5LB GPE	Triethyl phosphate	65	5.1	Li//LCO	0.2C cycling, 76.1% after 200 cycles	15

[g]GPE (PTFM)	FEC+EMC	~67.3	5.3	Li//NCM811	0.5C cycling, 75.6% after 280 cycles	16
[h]PTEM2	FEC	70	5.16	Li//LCO	1C cycling, 83.8% after 1000 cycles	17
[i]PPEGDA/ CMF	EC+DMC+D EC	~72	4.4	Li//LMFP	1C cycling, ~92% after 100 cycles	18
[j]DBPC-FS	EC+DMC+E MC	~73	4.6	Li//NCM811	1C cycling, 81.1% after 550 cycles	19
[k]MB-GPE	FEC + Methyl 2,2,2trifluoroethyl carbonate	~75	5.12 (>4.7 V)	Li//NCM811	0.5C cycling, 80.1% after 400 cycles	20
PTO-C9	EC+DEC+FE C	30	4.97 (4.6 V)	Li//NCM85	0.5C cycling, 73.3% after 450 cycles	This work

[a]FEC TFOA gel: The GPE with both FEC and *1H,1H,2H,2H*-tridecafluoro-n-octyl acrylate

[b]PCEE: Plastic-crystal-embedded elastomer electrolyte

[c]PP-LTPO CSE: Polyethylene glycol dimethyl ether- polymethyl methacrylate-$LiTa_2PO_8$ based composite solid-state electrolytes

[d]P(AEEO) based QSSE: Poly(2-(acryloyloxy)ethyl ethyl oxalate) based QSSE

[e]Fluorinated quasi-solid polymer electrolyte: Fluorinated quasi-solid polymer electrolyte incorporating HFA-MTFP-FEC-LiFSI

[f]35TFMA-0.5LF-0.5LB GPE: A GPE electrolyte that contains 60 vol% of trifluoroethyl methacrylate (TFMA) monomer in the precursor mixing with 0.2 M LiTFSI and 0.5 M LiDFOB

[g]GPE (PTFM): Poly (2,2,3,3-tetrafluoropropylmethacrylate) based gel polymer electrolyte

[h]PTEM2: Ethyl cyanoacrylate-based gel copolymer electrolyte

[i]PPEGDA/CMF: Poly[poly(ethylene glycol) diacrylate]/carbon nanotubes based electrolyte

[j]DBPC-FS: Polydouble-bond functionalized propylene carbonate–fluorostyrene based gel polymer electrolyte

[k]MB-GPE: Moderate Li^+-solvent binding GPE

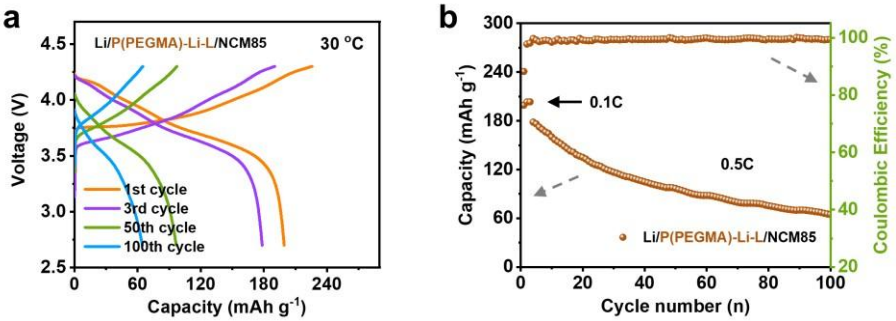

Fig. S55 Charge-discharge profiles of (a) Li/P(PEGMA)-Li-L/NCM85 at 30 °C and (b) the cycling stability of Li/P(PEGMA)-Li-L/NCM85 cell. L represents liquid: 30 wt% of EC+DEC+FEC (1:1:1, weight ratio).

Preparation of P(PEGMA) electrolytes: PEGMA (1.5 g), LiTFSI (1.034 g), liquid (EC+DEC+FEC) (1.086 g) in the (PEGMA+liquid):LiTFSI weight ratio of 2.5:1 and azodiisobutyronitrile (AIBN) (0.015 g) were added to glass bottle. This mixture was stirred for 30 mins at 30 °C and started to become sticky, which was then drop onto the glass-fiber membrane for further polymerization at 50 °C for 12 h.

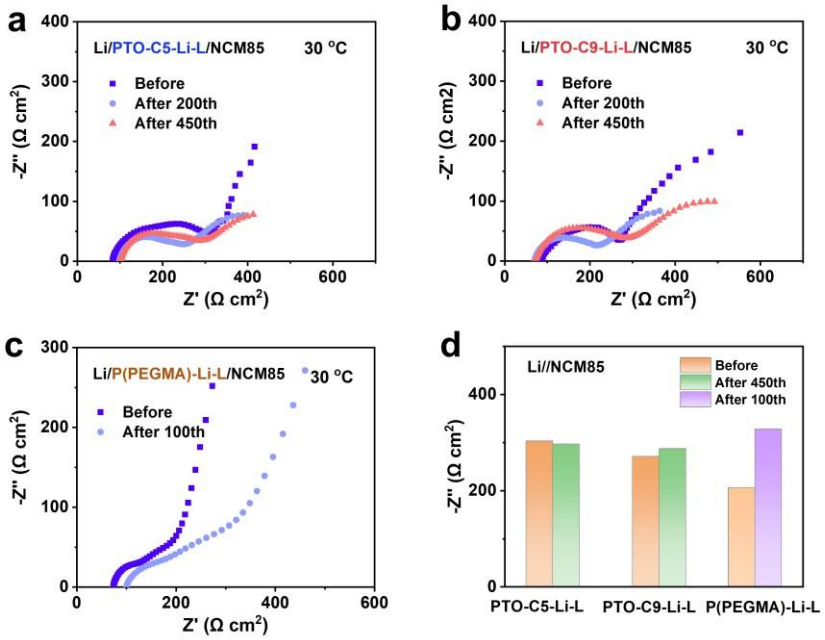

Fig. S56 The impedance curves of (a) Li/PTO-C5-Li-L/NCM85, (b) Li/PTO-C9-LiL/NCM85 and (c) Li/P(PEGMA)-Li-L/NCM85. (d) Impedance of Li//NCM85 cells with

different QSSEs before and after cycling. L represents liquid: 30 wt% of EC+DEC+FEC (1:1:1, weight ratio).

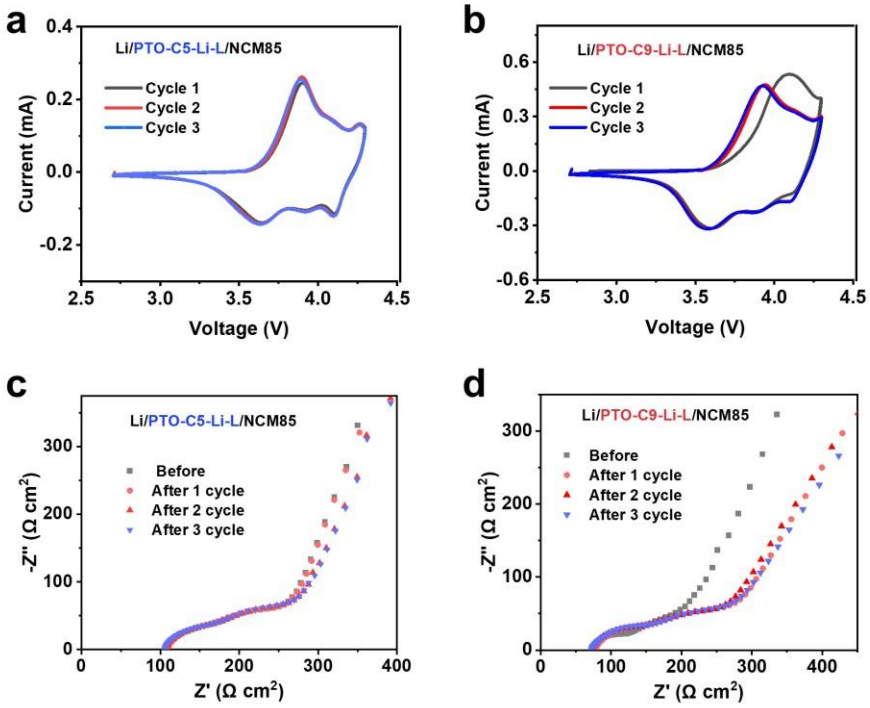

Fig. S57 CV curves of (a) Li/PTO-C5-Li-L/NCM85 and (b) Li/PTO-C9-Li-L/NCM85. Corresponding impedance curves of (c) Li/PTO-C5-Li-L/NCM85 and (d) Li/PTO-C9-LiL/NCM85. L represents liquid: 30 wt% of EC+DEC+FEC (1:1:1, weight ratio).

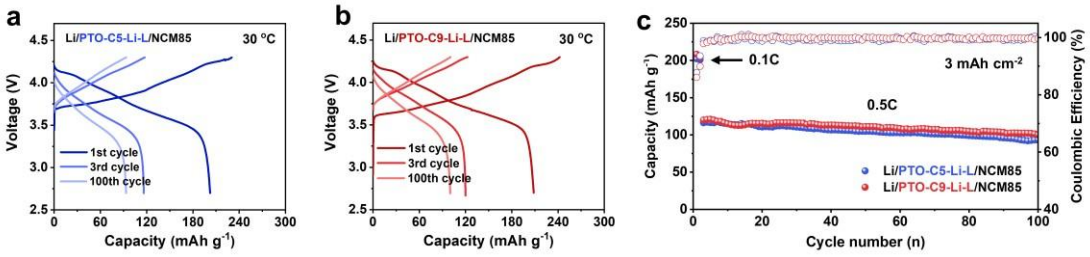

Fig. S58 Charge-discharge profiles of (a) Li/PTO-C5-Li-L/NCM85, (b) Li/PTO-C9-LiL/NCM85 at an area capacity of 3 mAh cm^{-2} and 0.5C. (c) The corresponding cycling stability. The Li foil is 100 μm and the negative/positive capacity (N/P) ratio is 6.9.

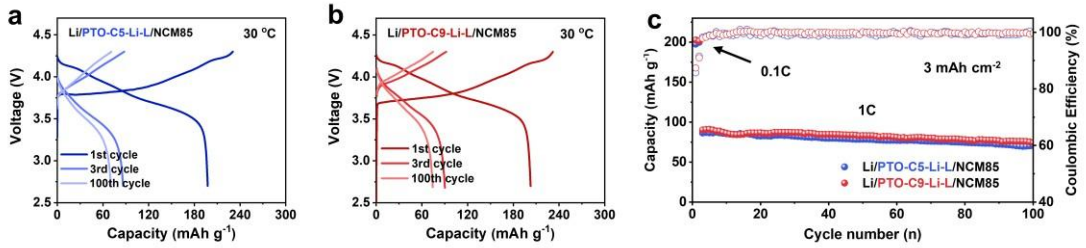

Fig. S59 Charge-discharge profiles of (a) Li/PTO-C5-Li-L/NCM85, (b) Li/PTO-C9-LiL/NCM85 at an area capacity of 3 mAh cm^{-2} and 1C. (c) The corresponding cycling stability. The Li foil is 100 μm and the N/P ratio is 6.9.

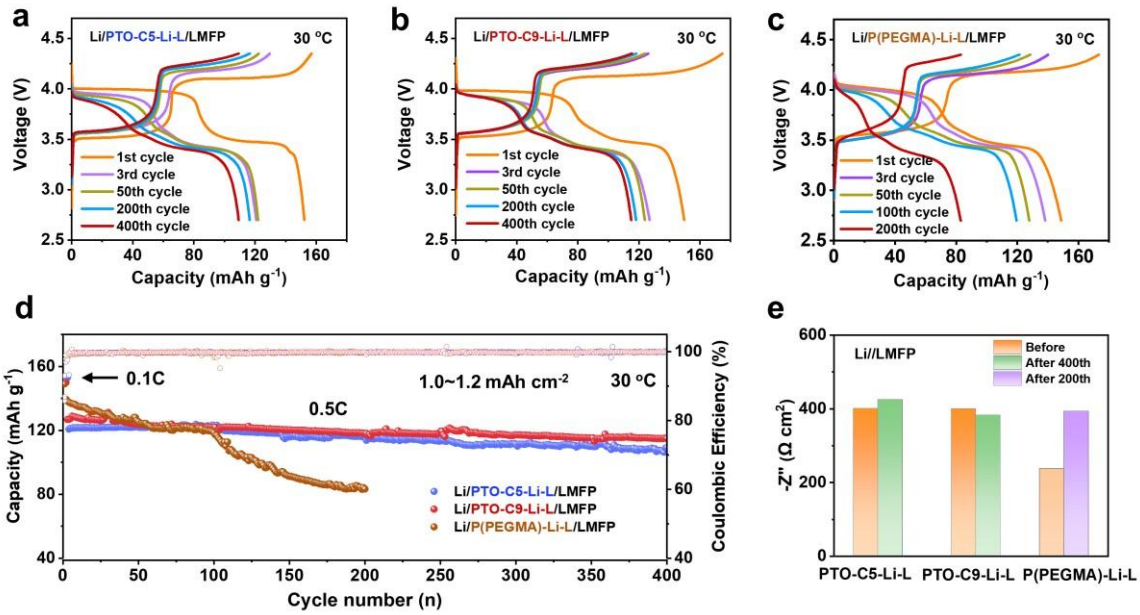

Fig. S60 Charge-discharge profiles of (a) Li/PTO-C5-Li-L/LMFP, (b) Li/PTO-C9-LiL/LMFP, (c) Li/P(PEGMA)-Li-L/LMFP at 30 °C and (d) the corresponding cycling stability of these three kinds of cells. (e) Impedance of Li//LMFP cells with different QSSEs before and after cycling. L represents liquid: 30 wt% of EC+DEC+FEC (1:1:1, weight ratio).

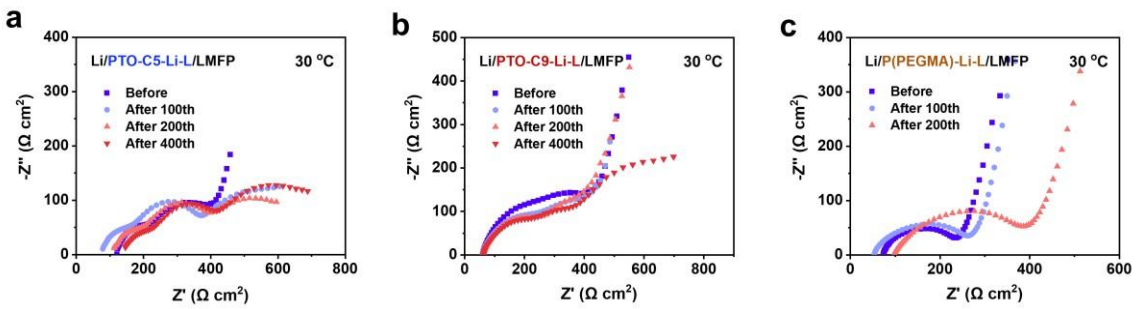

Fig. S61 The impedance curves of (a) Li/PTO-C5-Li-L/LMFP, (b) Li/PTO-C9-Li-L/LMFP,

(c) Li/P(PEGMA)-Li-L/LMFP after different cycles. L represents liquid: 30 wt% of EC+DEC+FEC (1:1:1, weight ratio).

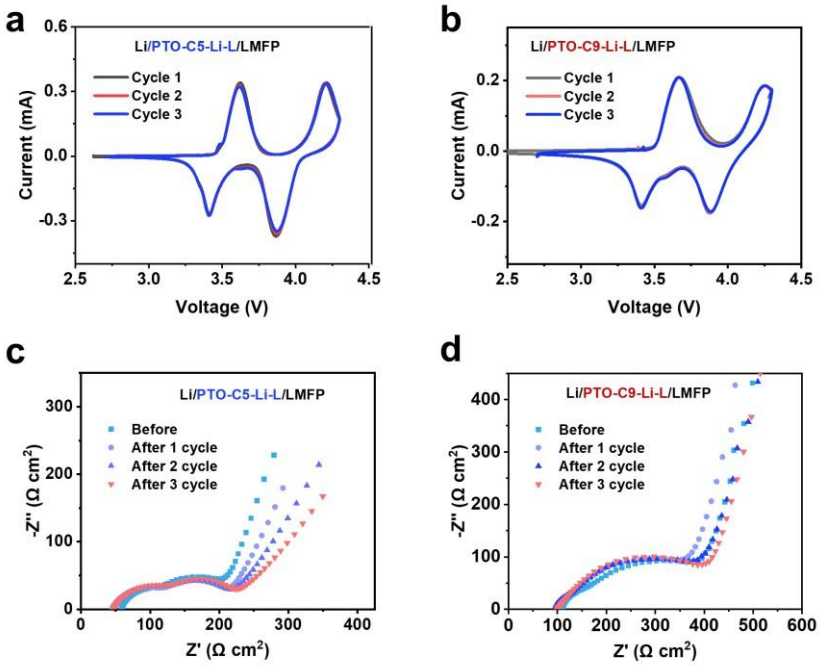

Fig. S62 CV curves of (a) Li/PTO-C5-Li-L/LMFP, (b) Li/PTO-C9-Li-L/LMFP.

Corresponding impedance curves of (c) Li/PTO-C5-Li-L/LMFP, (d) Li/PTO-C9-LiL/LMFP. L represents liquid: 30 wt% of EC+DEC+FEC (1:1:1, weight ratio).

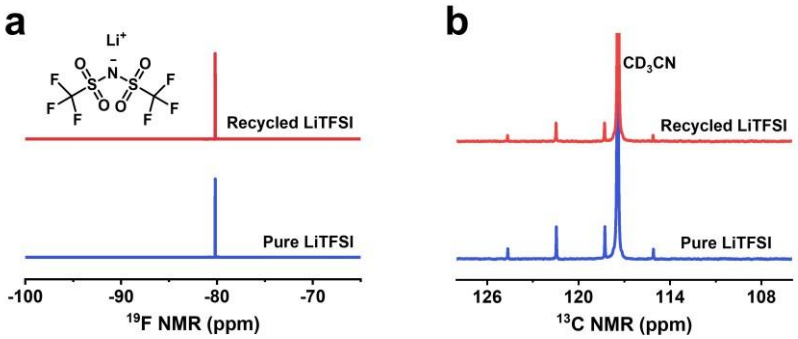

Fig. S63 (a) ^{19}F and (b) ^{13}C NMR spectra of pure LiTFSI and recycled LiTFSI.

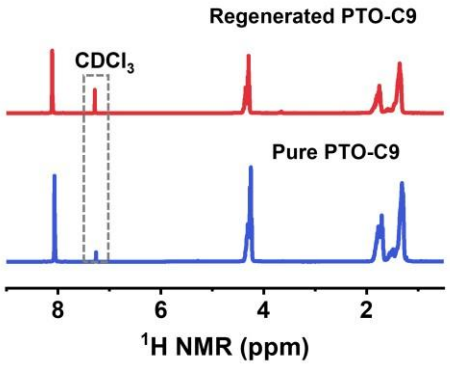

Fig. S64 ^{1}H NMR of regenerated PTO-C9 and fresh PTO-C9.

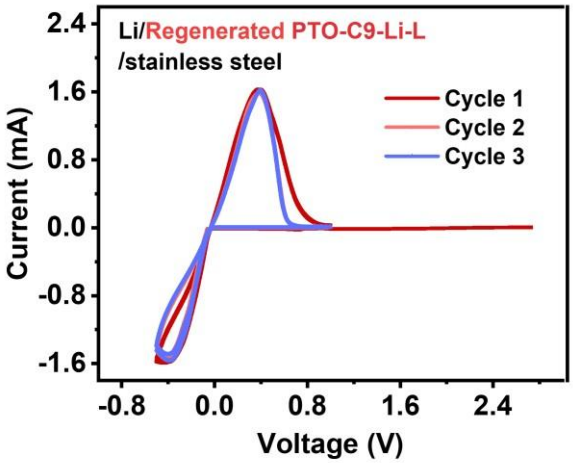

Fig. S65 CV curves of regenerated PTO-C9-Li-L in Li//stainless steel cells scanning from OCV to −0.5 V and then back to 1.0 V (25 °C). L represents liquid: 30 wt% of EC+DEC+FEC (1:1:1, weight ratio).

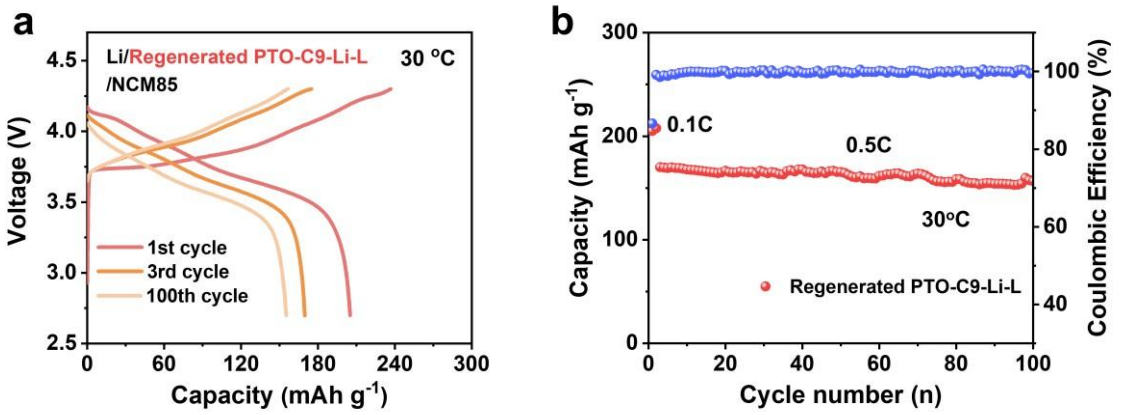

Fig. S66 (a) Charge-discharge profiles and (b) cycling performance of the Li//NCM85 cell using the regenerated PTO-C9-Li-L. The cell was charged-discharged at 0.1C for 2 cycles (formation cycles) and then runs at 0.5C. L represents liquid: 30 wt% of EC+DEC+FEC (1:1:1, weight ratio).

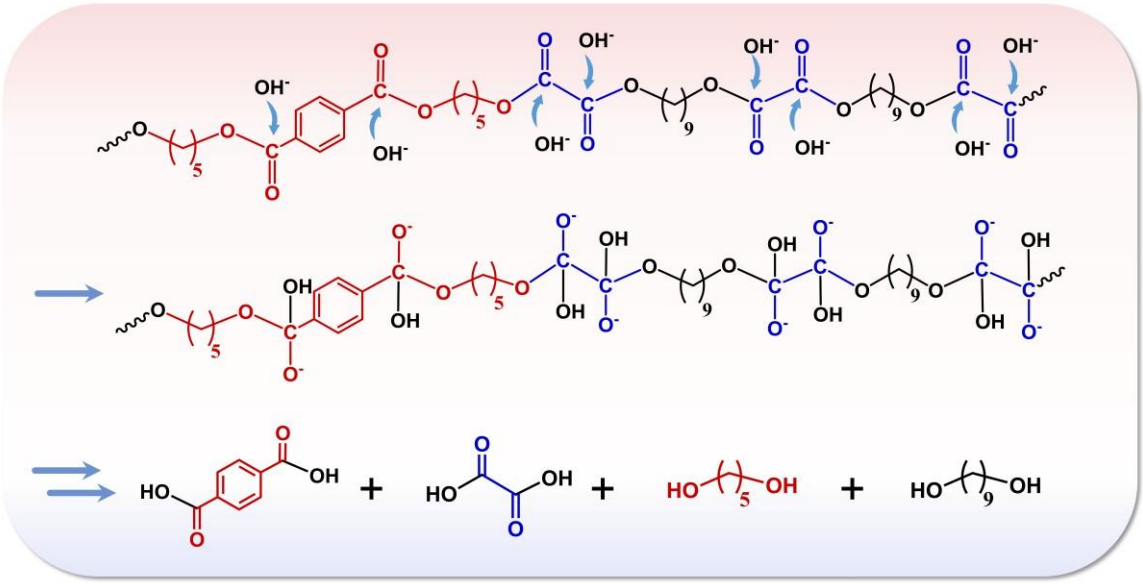

Fig. S67 The alkaline hydrolysis mechanism of PTO-C9.

References

1 M. J. Frisch, G. W. Trucks, H. B. Schlegel, G. E. Scuseria, M. A. Robb, J. R. Cheeseman, G. Scalmani, V. Barone, G. A. Petersson, H. Nakatsuji, X. Li, M. Caricato, A. V. Marenich, J. Bloino, B. G. Janesko, R. Gomperts, B. Mennucci, H. P. Hratchian, J. V. Ortiz, A. F. Izmaylov,

J. L. Sonnenberg, D. Williams-Young, F. Ding, F. Lipparini, F. Egidi, J. Goings, B. Peng, A. Petrone, T. Henderson, D. Ranasinghe, V. G. Zakrzewski, J. Gao, N. Rega, G. Zheng, W. Liang, M. Hada, M. Ehara, K. Toyota, R. Fukuda, J. Hasegawa, M. Ishida, T. Nakajima, Y. Honda, O. Kitao, H. Nakai, T. Vreven, K. Throssell, J. A. Montgomery, Jr., J. E. Peralta, F. Ogliaro, M. J. Bearpark, J. J. Heyd, E. N. Brothers, K. N. Kudin, V. N. Staroverov, T. A. Keith, R. Kobayashi, J. Normand, K. Raghavachari, A. P. Rendell, J. C. Burant, S. S. Iyengar, J. Tomasi, M. Cossi, J. M. Millam, M. Klene, C. Adamo, R. Cammi, J. W. Ochterski, R. L. Martin, K. Morokuma, O. Farkas, J. B. Foresman and D. J. Fox, *Gaussian, Inc., Wallingford CT*, 2016.

2 A. D. Becke, *J. Chem. Phys.*, 1993, **98**, 5648–5652.

3 C. Lee, W. Yang and R. G. Parr, *Phys. Rev. B.*, 1998, **37**, 785.

4 M. J. Abraham, T. Murtola, R. Schulz, S. Páll,J. C. Smith, B. Hess and E. Lindahl, *SoftwareX*, 2015, **1-2,** 19–25.

5 G. A. Kaminski, R. A. Friesner and J. Tirado-Rives, *J. Phys. Chem. B.*, 2001, **105**, 6474–6487.

6 C. I. Bayly, P. Cieplak, W. Cornell and P. A. Kollman, *J. Phys. Chem.*, 1993, **97**, 10269–10280.

7 T. Lu and F. Chen, *J. Comput. Chem.*, 2012, **33**, 580–592.

8 V. V. Chaban and I. V. Voroshylova, *J. Phys. Chem. B.*, 2015, **119**, 6242–6249.

9 L. Martínez, R. Andrade, E. G. Birgin and J. M. Martínez, *J. Comput. Chem*., 2009, **30**, 2157–2164.

10 M. Li, D. A. Rakov, Y. Fan, C. Wang, C. Wang, J. A. Yuwono, S. Xia, J. Mao and Z. Guo, *Angew. Chem. Int. Ed.*, 2025, **64**, e202513450.

11 M. J. Lee, J. Han, K. Lee, Y. J. Lee, B. G. Kim, K.-N. Jung, B. J. Kim and S.-W. Lee, *Nature*, 2022, **601**, 217–222.

12 R.-A. Tong, Y. Huang, C. Feng, Y. Dong and C.-A. Wang, *Adv. Funct. Mater*., 2024, **34**, 2315777.

13 P. Li, J. Hao, S. He, Z. Chang, X. Li, R. Wang, W. Ma, J. Wang, Y. Lu, H. Li, L. Zhang and W. Zhou, *Nat. Commun*. 2025, **16**, 3727.

14 Z. Li, W. Li, Z. Li, X. Guo, J. Fu, Q. Chen and H. Yang, *Nat. Commun*. 2025, **16**, 9265.

15 Q. Sun, Z. Gong, T. Zhang, J. Li, X. Zhu, R. Zhu, L. Wang, L. Ma, X. Li, M. Yuan, Z. Zhang, L. Zhang, Z. Qian, L. Yin, R. Ahuja and C. Wang, *Nano-Micro Lett*. 2025, **17**, 18.

16 Q. Zhang, T. Bian, X. Wang, R. Shi and Y. Zhao, *Angew. Chem. Int. Ed*., 2025, **64**, e202415343.

17 W. Min, L. Li, M. Wang, S. Ma, H. Feng, W. Wang, H. Ding, T. Cheng, Z. Li, T. Saito, H. Yang and P.-F. Cao, *Angew. Chem. Int. Ed*., 2025, **64**, e202422510.

18 L. Nie, R. Gao, M. Zhang, Y. Zhu, X. Wu, Z. Lao and G. Zhou, *Adv. Energy. Mater*., 2024, **14**, 2302476.

19 W. Deng, H. Xu, J. Yu, A. Xu, L. Shi, Z. Xiao, W. Zhang, C. He and L. Xu, *Angew. Chem. Int. Ed*., 2026, **65**, e17516.

20 S. Zhang, Z. Li, Y. Zhang, X. Wang, P. Dong, S. Lei, W. Zeng, J. Wang, X. Liao, X. Chen, D. Li and S. Mu, *Energy Environ. Sci.*, 2025, **18**, 3807–3816.